An siRNA screen for ATG protein depletion reveals the extent of the unconventional functions of the autophagy proteome in virus replication

Mario Mauthe,[1,2] Martijn Langereis,[4] Jennifer Jung,[5] Xingdong Zhou,[1,6] Alex Jones,[1,2] Wienand Omta,[2] Sharon A. Tooze,[7] Björn Stork,[8] Søren Riis Paludan,[9] Tero Ahola,[10] Dave Egan,[2] Christian Behrends,[5] Michal Mokry,[3,11] Cornelis de Haan,[4] Frank van Kuppeveld,[4] and Fulvio Reggiori[1,2]

[1]Department of Cell Biology, University Medical Center Groningen, University of Groningen, 9713 AV Groningen, Netherlands
[2]Department of Cell Biology and [3]Regenerative Medicine Center Utrecht, Center for Molecular Medicine, University Medical Center Utrecht, 3584 CX Utrecht, Netherlands
[4]Virology Division, Department of Infectious Diseases and Immunology, Utrecht University, Utrecht, 3584 CL Utrecht, Netherlands
[5]Institute of Biochemistry II, Goethe University School of Medicine, 60590 Frankfurt am Main, Germany
[6]Department of Preventive Veterinary Medicine, College of Veterinary Medicine, Northeast Agricultural University, Harbin, Heilongjiang 150030, People's Republic of China
[7]Lincoln's Inn Fields Laboratories, The Francis Crick Institute, London WC2A 3LY, England, UK
[8]Institute of Molecular Medicine I, Heinrich-Heine-University, 40225 Düsseldorf, Germany
[9]Department of Biomedicine, University of Aarhus, 8000 Aarhus C, Denmark
[10]Department of Food and Environmental Sciences, University of Helsinki, 00014 Helsinki, Finland
[11]Division of Pediatrics, Wilhelmina Children's Hospital, University Medical Center Utrecht, 3584 EA Utrecht, Netherlands

Autophagy is a catabolic process regulated by the orchestrated action of the autophagy-related (ATG) proteins. Recent work indicates that some of the ATG proteins also have autophagy-independent roles. Using an unbiased siRNA screen approach, we explored the extent of these unconventional functions of ATG proteins. We determined the effects of the depletion of each ATG proteome component on the replication of six different viruses. Our screen reveals that up to 36% of the ATG proteins significantly alter the replication of at least one virus in an unconventional fashion. Detailed analysis of two candidates revealed an undocumented role for ATG13 and FIP200 in picornavirus replication that is independent of their function in autophagy as part of the ULK complex. The high numbers of unveiled ATG gene-specific and pathogen-specific functions of the ATG proteins calls for caution in the interpretation of data, which rely solely on the depletion of a single ATG protein to specifically ablate autophagy.

Introduction

Macroautophagy (hereafter referred to as autophagy) is an evolutionarily conserved transport pathway required for the degradation of long-lived proteins and organelles and thus is essential for the maintenance of cell homeostasis (Levine and Klionsky, 2004; Shintani and Klionsky, 2004; Mizushima et al., 2008). Autophagy is characterized by the formation of double-membrane vesicles called autophagosomes that sequester cytoplasmic components and deliver them into lysosomes (Levine and Klionsky, 2004; Kawamata et al., 2008). Autophagy is active at basal level in every eukaryotic cell and can be enhanced by several cellular stresses, including nutrient starvation (Kroemer et al., 2010) or pathogen invasions (Levine et al., 2011). Autophagosome biogenesis is orchestrated by the autophagy-related (ATG) proteins, which have been subdivided in functional clusters of genes mainly based on physical interactions (He and Klionsky, 2009). One of them is the ULK complex, which consists of the ULK1 (or ULK2) kinase, ATG13, FIP200, and ATG101, and it is at the terminus of several signaling cascades that positively or negatively regulate autophagy (Wong et al., 2013). Stimulation of ULK1 activity initiates the assembly of the autophagy machinery at the site where autophagosomes will emerge, which is often in close proximity of the ER (Axe et al., 2008). This assembly involves the recruitment of additional functional clusters of proteins, including ATG9A and an autophagy-specific phosphatidylinositol 3-kinase complex class III (Yang and Klionsky, 2010), that generates phosphatidylinositol-3-phosphate on autophagosomal membranes, promoting the

Correspondence to Fulvio Reggiori: f.m.reggiori@umcg.nl

M. Langereis' present address is Discovery and Technology Research, MSD Animal Health, 5831 AN Boxmeer, Netherlands.

Abbreviations used: APSM, average peptide spectral match; CV, coxsackievirus B3; EBSS, Earle's balanced salt solution; EMCV, encephalomyocarditis virus; HSV, herpes simplex virus; IAV, influenza A virus; IRES, internal ribosome entry site; MEF, mouse embryonic fibroblast; MHV, mouse hepatitis virus; MS, mass spectrometry; SFV, Semliki Forest virus; SF, soluble fraction; VaV, vaccinia virus.

The Rockefeller University Press $30.00
J. Cell Biol. Vol. 214 No. 5 619–635
www.jcb.org/cgi/doi/10.1083/jcb.201602046

binding of other ATG factors such as the WIPI proteins (Mari et al., 2011). Subsequently two ubiquitin-like conjugation systems are recruited to elongate and close the initial precursor cistern, the phagophore, to form an autophagosome (Yang and Klionsky, 2010).

It has long been believed that the ATG proteome is exclusively involved in autophagy, and thus a multitude of studies on the physiological and pathological roles of autophagy have relied on the ablation of a single ATG gene. Recent findings, however, have indicated that ATG genes or functional clusters of *ATG* genes fulfill important cellular functions outside the context of their role in autophagy, some of which are involved in pathogen–host interaction (Bestebroer et al., 2013; Subramani and Malhotra, 2013).

To get an overall view of the extent of the unconventional functions of ATG proteins, we decided to explore the relevance of single and redundant ATG genes in the replication of six viruses belonging to different virus families: herpes simplex virus-1 (HSV-1), vaccinia virus (VaV), Semliki Forest virus (SFV), mouse hepatitis virus (MHV), encephalomyocarditis virus (EMCV) and influenza A virus (IAV). Although a block of autophagy was not altering virus replication in most of the tested infections, a considerable number of single protein depletions inhibited or enhanced the replication of one or more viruses. As a proof of principle, we examined the role of ATG13 and FIP200 in picornaviral infection and demonstrated that these proteins control the replication of members of this virus family outside the context of the ULK complex. Moreover RNA-sequencing analyses highlighted potential proteins and cellular pathways through which ATG13 and FIP200 could influence picornaviral infection independently of autophagy. Altogether, our results reveal that an unpredicted large number of ATG genes have an unconventional function and therefore strongly challenge the current notion that depletion of an ATG gene leads principally to a specific block of autophagy.

Results

ATG proteome-specific siRNA screen identifies unconventional roles of ATG proteins in viral replication

We generated a custom siRNA library that targeted all ATG proteins individually to identify novel unconventional functions of the ATG proteins acting outside the context of autophagy (Fig. 1 and Table S1). Because some ATG proteins have partially or totally redundant functions in autophagy (for example, ATG2A and ATG2B; Velikkakath et al., 2012), specific sets of *ATG* genes were also simultaneously targeted (Table S2). To avoid cell-specific functions, which could explain some of the inconsistent results in the literature (Zhang et al., 2011; Chakrabarti et al., 2012; Tabor-Godwin et al., 2012), and focus on key proteins relevant to the virus life cycle in all cell types, we performed the siRNA screen in two cell lines: HeLa and U2OS cells. We chose HeLa and U2OS cells because they originate from diverse tissues, i.e., cervix and bone tissue, respectively (Scheffner et al., 1991; Landers et al., 1997). For the whole screen, we used HeLa cells expressing the mCeaCam1 surface protein, which is required to allow efficient infection by MHV (Burkard et al., 2014). For the same reason, HEK293T cells expressing mCeaCam1 (Wicht et al., 2014) were used instead of U2OS cells as the second cell line for the screen with MHV.

We controlled the effectiveness of the ATG gene knockdown by first measuring the inhibition of autophagy through the assessment of endogenous p62 puncta formation (Fig. 1, B and D; Klionsky et al., 2016). p62 is a well-known substrate of autophagy and accumulates in discrete punctate cytoplasmic aggregates when this degradative pathway is impaired (Klionsky et al., 2016). We found that the number of p62 puncta per cell was increased in the majority of the ATG-depleted cells in both HeLa and U2OS cell lines (Fig. 1 B and Table S5), indicating that autophagic degradation is blocked. ATG7 and ULK1 depletions were among the strongest increasers of p62 puncta (Chan et al., 2007), whereas p62 depletion led to a decrease in p62 puncta per cell. To reinforce this finding, we also measured endogenous LC3 puncta number and area (Fig. 1 D and Fig. S1 A; Klionsky et al., 2016). Consistently with the literature, these analyses revealed two populations of ATG proteins that upon deletion lead to either a reduction or increase of LC3 puncta formation (Fig. 1 D, Fig. S1 A, and Table S5). Proteins such as ATG5, ATG12, or WIPI2 that are known to be involved in LC3 recruitment onto autophagosomal membranes reduce LC3 puncta formation (Mizushima et al., 2001; Polson et al., 2010). Conversely, we found an increase in LC3 puncta number in cells lacking proteins like WIPI4 and ATG2 that lead to an accumulation of autophagosomal intermediates positive for LC3 (Lu et al., 2011; Velikkakath et al., 2012). Altogether, these verification experiments confirmed that our siRNA library and the used screening protocol are effective in blocking the autophagy function of the targeted genes in both cell lines.

For the screen, we used luciferase-expressing virus strains and monitored luciferase expression as a readout for their replication (Fig. 1 A). The screen was independently run four times in each cell line and for each virus and was controlled by internal positive controls (see Materials and methods; Fig. 1 C). In contrast to the autophagy measurement in which an accumulation of p62 puncta was detected in the large majority of the samples (Fig. 1, B and D; and Table S5), we did not observe a uniform redistribution of the changes in replication in both tested cell lines in any of the examined viruses (Fig. S1 B and Fig. S2), even if HSV-1 replication was to some extent reduced in 75% of the tested ATG protein knockdown cells. Our data in particular showed that autophagy does not play a role in either inhibiting or promoting the replication of EMCV, IAV, and MHV (Figs. 1 D, S1 B, and S2). The results for VaV and SFV, however, differed from the ones obtained with the other viruses. We observed an almost uniform increase in viral replication upon ATG gene depletion in HeLa cells, suggesting a possible function of autophagy in repressing VaV and SFV infection. In contrast, VaV and SFV replication was almost uniformly decreased upon ATG gene knockdown in U2OS cells, indicating a beneficial role of autophagy. The prominent cell-specific differences in the VaV and SFV replication–autophagy interaction could explain some of the discrepancies in the literature about the role of autophagy in specific types of infections and highlight the importance of using more than one cell line when studying this relationship.

Overall, the knockdown of 16 out of 44 tested ATG proteins (36% of the whole ATG proteome) caused a significant change in viral replication in one or more viruses independently of the cell line (Fig. 1, C and D; Fig. S1 B; and Fig. S2). No single gene was identified that regulates viral replication of all the tested viruses, but rather particular ATG genes influenced the replication of a particular virus (Fig. 1 D). These data show

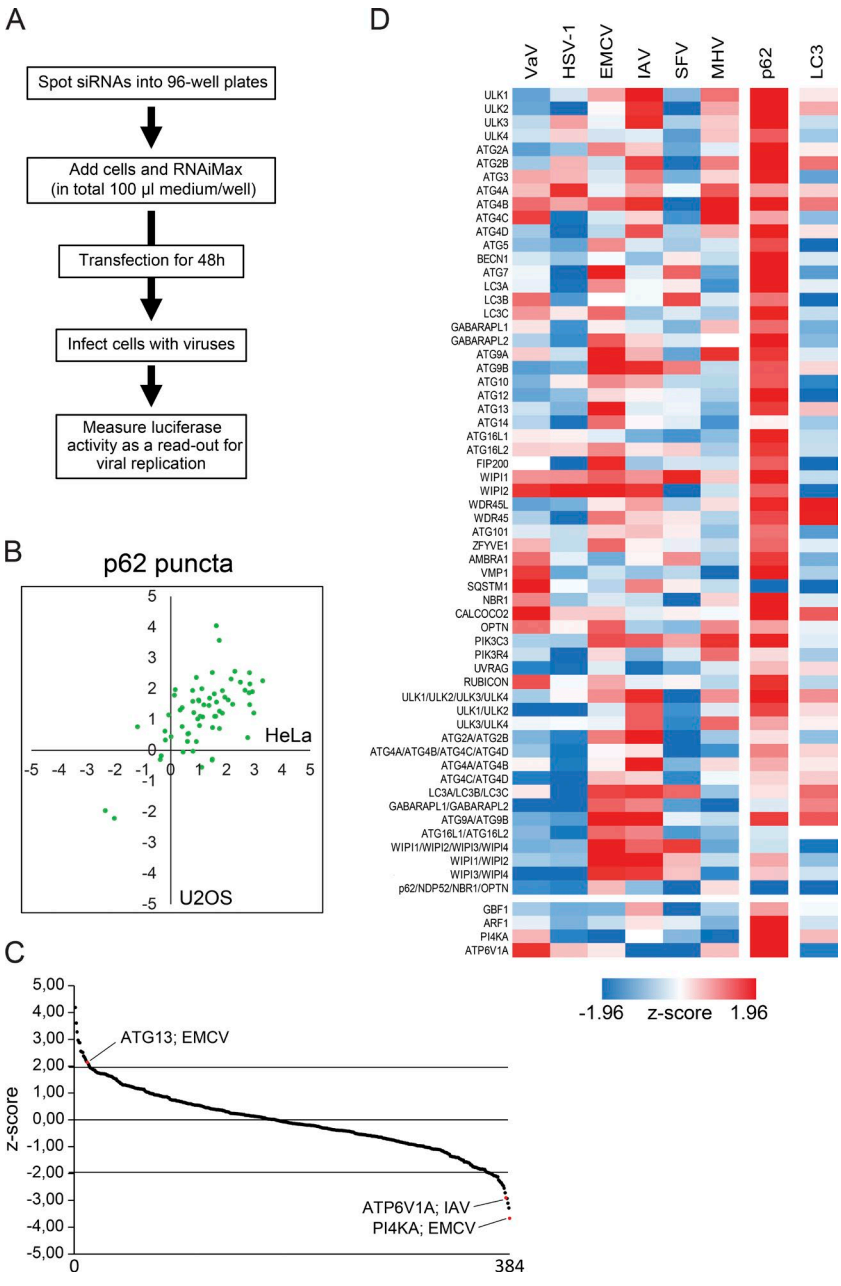

Figure 1. **An ATG proteome-specific siRNA screen identifies unconventional roles of ATG proteins in viral replication.** (A) Schematic overview of the siRNA-based screen workflow. (B) U2OS and HeLa-mCea-Cam1 cells were transfected with a customized ATG-specific siRNA library (Tables S1 and S2), and endogenous p62 and LC3 puncta were automatically counted. Z-scores of p62 puncta measurements are presented in a scatterplot, where the data obtained in HeLa cells are ranked on the x axis and those acquired in U2OS cells are on the y axis. (C) The combined Z-scores of viral replication measurements (y axis) for all viruses and cell lines are plotted on a single graph. The dotted black lines indicate the location of the measurements that are significantly different in comparison to the control. Arrows highlight the results for two examples of genes known to be essential for virus replication (ATP6V1A for IAV and PI4KA for EMCV) and ATG13, a newly found replication suppressor for EMCV. (D) Heatmap of the siRNA screen where the combined Z-scores of both cell lines for the viral replication and p62 puncta measurement are indicated as well as the Z-scores for LC3 puncta in U2OS cells. Red indicates an enhancement in viral replication, p62, or LC3 accumulation in puncta, whereas blue underlines inhibition of viral replication or a decrease in the number of p62- or LC3-positive puncta (n = 4 for viral infection and LC3 puncta assessment; n = 3 for p62 puncta quantification).

that ATG genes have several fundamentally important ATG gene-specific, cell line–specific, and pathogen-specific roles.

ATG13 and FIP200 control EMCV and CV replication independently from their autophagy function as part of the ULK complex

To validate the overall outcome of the screen, we focused on ATG13. Unlike the other ULK complex components, its depletion caused a significant increase in EMCV replication (Fig. 1, C and D). We first determined the efficiency of ATG13 knockdown at the mRNA and protein level by quantitative real-time PCR and Western blot. ATG13 was completely depleted from cells by at least three out of four single siRNA probes composing the pool used in the screen (Fig. S3, A and B; and Table S3). We then reassessed the replication of the studied virus in both U2OS and HeLa cells with the siRNA that was very efficiently depleting ATG13 (i.e., probe 4) to exclude possible off-target effects of a mixture of probes. We also included another member of the picornavirus family, coxsackievirus B3 (CV; member of the Enterovirus B species), which has a pathological impact on human health (Muehlenbachs et al., 2015). In agreement with the screen results (Fig. 1), replication of HSV-1, IAV, VaV, and SFV were not affected by ATG13 depletion, whereas EMCV was enhanced (Fig. S4). Interestingly CV replication was significantly augmented in both cell lines upon ATG13 depletion (Fig. S4). Enhanced CV and EMCV replication was confirmed in immortalized *ATG13*$^{-/-}$ mouse embryonic fibroblasts (MEFs) complemented or not with a plasmid carrying *ATG13* (Hieke et al., 2015; Fig. 2, A–C). We also measured an increase in IAV replication in *ATG13*$^{-/-}$ MEFs, but this is very likely a cell line–specific effect, because it was not observed in U2OS or HeLa cells (Fig. 2 A).

ATG13 carries out its function in autophagy as part of the ULK complex (Wong et al., 2013), and therefore, we verified

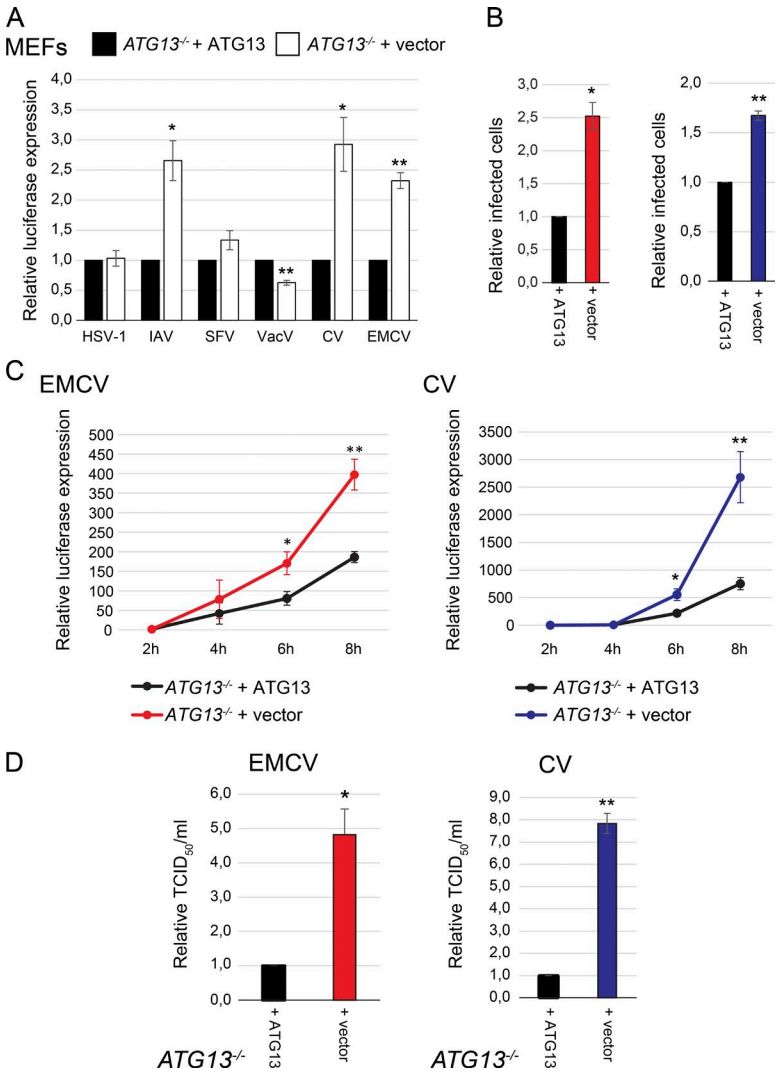

Figure 2. **Viral replication of EMCV and CV is enhanced in *ATG13*$^{-/-}$ MEFs cells.** (A) *ATG13*$^{-/-}$ MEFs retrovirally transformed with either an empty vector or one expressing HA-ATG13 were infected with the indicated luciferase expressing viruses for 6 h before measuring luciferase expression (n = 4). (B) *ATG13*$^{-/-}$ MEFs retrovirally transformed with either an empty vector or one carrying HA-ATG13 were infected with EMCV or CV, cells were stained using antibodies against viral proteins, and the number of infected cells was determined by automated counting of immunofluorescence images (n = 3). (C) *ATG13*$^{-/-}$ MEFs retrovirally transformed with either an empty vector or one expressing HA-ATG13 were infected with luciferase-expressing EMCV or CV for 2, 4, 6, and 8 h before measuring luciferase expression (n = 6 for EMCV and n = 8 for CV). (D) EMCV and CV titer was determined in *ATG13*$^{-/-}$ MEFs retrovirally transformed with either an empty vector or one expressing HA-ATG13 using the tissue culture infectious dose ($TCID_{50}$) assay (n = 3). All data are presented relative to the control at 0 h (folds). Error bars represent SEM. *, $P < 0.05$; **, $P < 0.01$; no symbol indicates not significant.

whether, as indicated by the screen results (Fig. 1), the rest of the subunits do not affect the replication of EMCV and CV. We first selected single siRNAs that were efficiently knocking down ULK1, ULK2, FIP200, and ATG101 and ATG7, a key autophagy protein (Mizushima et al., 1998) that is not part of the ULK complex by quantitative real-time PCR and/or Western blot (Fig. S3). This examination revealed that the levels of these proteins were reduced to a similar extent in both tested cell lines. However, we observed differences in the knockdown efficiency in the tested cell lines when analyzed by quantitative real-time PCR in samples treated with the siRNA pool targeting FIP200. This difference in knockdown efficiency within cell lines might also add to the variation in virus replication observed in the screen for some genes. As documented previously (Mizushima et al., 1998; Chan et al., 2007; Hara et al., 2008; Hosokawa et al., 2009; Jung et al., 2009; Ro et al., 2013), depletion of these proteins blocked autophagy. We measured the autophagic flux block using the long-lived protein degradation assay (Chan et al., 2007) and accumulation of endogenous p62 puncta (Fig. 3). This result proved that all used single siRNAs effectively block the canonical function of the targeted proteins in autophagy under the knockdown conditions used to test viral replications.

We verified that autophagy does not increase EMCV and CV replication by depletion of ATG7 (Mizushima et al., 1998) or treatment with the autophagy inhibitor wortmannin (Blommaart et al., 1997). We also confirmed that knockdown of the ULK complex components had no effect on EMCV and CV replication, with the exception of FIP200 (Fig. 4, A–F; and Fig. 5, A and C), which already displayed higher, but not significant, EMCV replication in the screen (Fig. 1 D; see Table S5). We also corroborated these results in HEK293T cells in which the knockdown of ATG13 and FIP200 enhanced the number of CV infected cells whereas that of ATG7 did not (Fig. 6, A and B). Furthermore, overexpression of ATG13 or FIP200 in doxycycline-inducible stable HEK293T cells (Fig. 6, F, G, I, and J) reduced the number of CV-infected cells. Although nutrient starvation increased phosphorylation of ATG13 by ULK1, which elicits autophagy stimulation (Hieke et al., 2015), there were no changes in ATG13 phosphorylation upon infection with EMCV or CV (Fig. 4 G). The notion that the ULK complex is not activated during EMCV and CV infection was reinforced by analyzing the activity of mTORC1 using S6 protein phosphorylation as the readout (Wong et al., 2013; Fig. 4 H). Importantly, EMCV and CV infections in the presence or absence of ATG13 did not influence mTORC1 activity (Fig. 4 H). Altogether, these results demonstrate that ATG13 and FIP200 are involved in the control of EMCV and CV replication, whereas the ULK complex, and generally autophagy, are not required for this function.

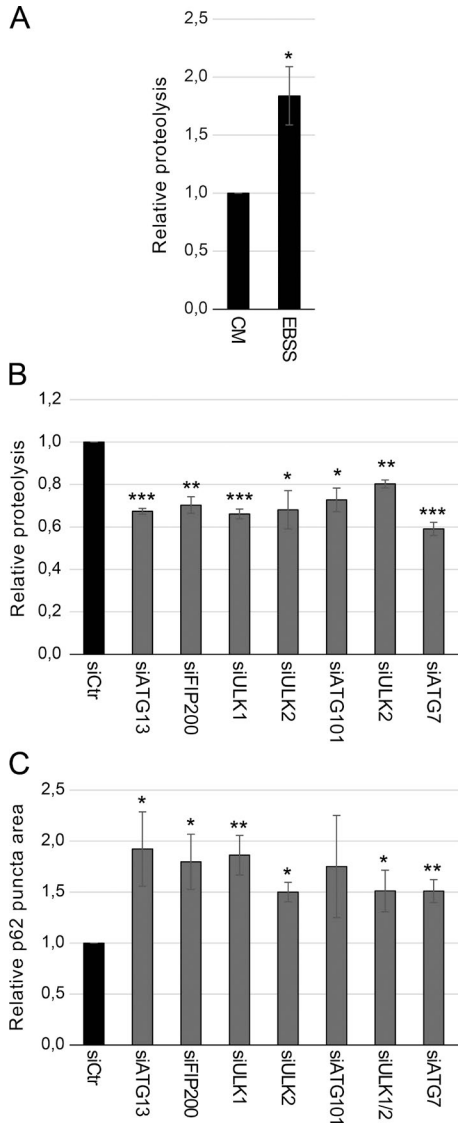

Figure 3. **Knockdown of the ULK complex components inhibit autophagic flux.** (A) U2OS cells transfected with control siRNA were nutrient-starved for 2 h (EBSS) or left in culture medium (CM) before determining the percentage of degraded long-lived proteins (n = 6). (B) The indicated genes were depleted in U2OS cells, and long-lived protein degradation was measured upon 2 h of amino acid starvation (n = 4). (C) The indicated genes were depleted in U2OS cells before automatically quantify the endogenous p62 puncta (n = 3). All data are presented relative to the control (folds). Error bars represent SEM. *, P < 0.05; **, P < 0.01; ***, P < 0.001; no symbol indicates not significant. siCtr, scramble siRNA.

Next, we explored whether ATG13 and FIP200 control EMCV and CV replication through the same or different pathways. Simultaneous knockdown of ATG13 and FIP200 did not increase virus replication (Fig. 4, A and B; and Fig. 5, A and C) compared with the single depletions, nor did it lead to an enhanced cell lysis (Fig. 5, B and D). This observation indicates that ATG13 and FIP200 act together in the control of EMCV and CV replication. Finally, depletion of ATG13 or FIP200 still increased EMCV and CV infection in ATG7-depleted cells, reinforcing the notion of an unconventional function of these two proteins outside the context of autophagy (Fig. 4, A–F; and Fig. 5).

ATG13 depletion enhances EMCV and CV replication, but not virus cell entry

An increase in EMCV and CV replication upon gene depletion could reflect a direct involvement of ATG13 or FIP200 in genome replication of the viruses or in their cell entry. Picornaviruses are positive-stranded RNA viruses, and their replication within the cell starts from their genomic viral RNA (Baron and Baltimore, 1982). Depletion of ATG13 significantly increased EMCV and CV replication from their transfected viral RNA compared with the control (Fig. 7, A and C), indicating that it is unlikely that ATG13 has a role in virus entry. Upon specific inhibition of EMCV and CV genomic RNA replication with GPC-N114 (van der Linden et al., 2015) and guanidine hydrochloride (De Palma et al., 2008), respectively, no difference in luciferase levels was observed, indicating that depletion of ATG13 does not affect viral RNA translation. To further rule out that ATG13 depletion modifies internal ribosome entry site (IRES)–dependent (Muthukrishnan et al., 1975) or cap-dependent translation (Pelletier and Sonenberg, 1988), we measured IRES- and cap-dependent luciferase-based reporter activity in control and ATG13-depleted cells (Fig. 7, E and F). We did not observe a general enhancement of cap-dependent protein translation or IRES-mediated translation upon ATG13 depletion (Fig. 7, E and F). We thus concluded that ATG13, and by extension FIP200, are directly involved in EMCV and CV genome replication.

To further test whether ATG13 depletion has also a role in virus entry, we infected control and ATG13 knockdown U2OS cells with EMCV or CV luciferase-carrying strains before adding GPC-N114 and guanidine hydrochloride, respectively, to inhibit replication. As expected, ATG13 depletion increased EMCV and CV luciferase expression compared with the control (Fig. 7, B and D). Addition of the replication inhibitors 1 h after virus inoculation blocked EMCV- or CV-mediated luciferase expression to the same extent in control cells and ATG13-depleted cells (Fig. 7, B and D). This shows that the amount of genomic RNA that enters the cells upon EMCV or CV infection is similar in presence or absence of ATG13, arguing against a role in virus entry.

Depletion of ATG13 and FIP200 results in higher picornavirus production in host cells

Next, we explored whether the enhanced EMCV and CV replication observed upon depletion of ATG13 or FIP200 also resulted in higher virus production (Figs. 6 and 8). Infecting ATG13- or FIP200-depleted cells with either EMCV or CV led to a significant reduction in the percentage of surviving cells compared with the control or any other ULK complex component (Fig. 6 C and Fig. 8, A and C). Analysis of the infective virions released from the cells revealed that the virus titers were increased twofold to fivefold in ATG13- or FIP200-depleted cells compared with control cells, which was not observed when other ULK complex components or ATG7 were knocked down (Fig. 6 D and Fig. 8, B and D). A higher virus titer for EMCV and CV was also observed in *ATG13*$^{-/-}$ MEFs (Fig. 2 D). Conversely, doxycycline-induced overexpression of ATG13 or FIP200 reduced the CV titer in HEK293T cells compared with the noninduced control cells (Fig. 6, E, H, and K).

We furthermore investigated whether these two proteins also control infections caused by other members of the picornavirus family: enterovirus 71 (EV71; member of the EV-A species; Bible et al., 2007), coxsackievirus A21 (CVA21; member

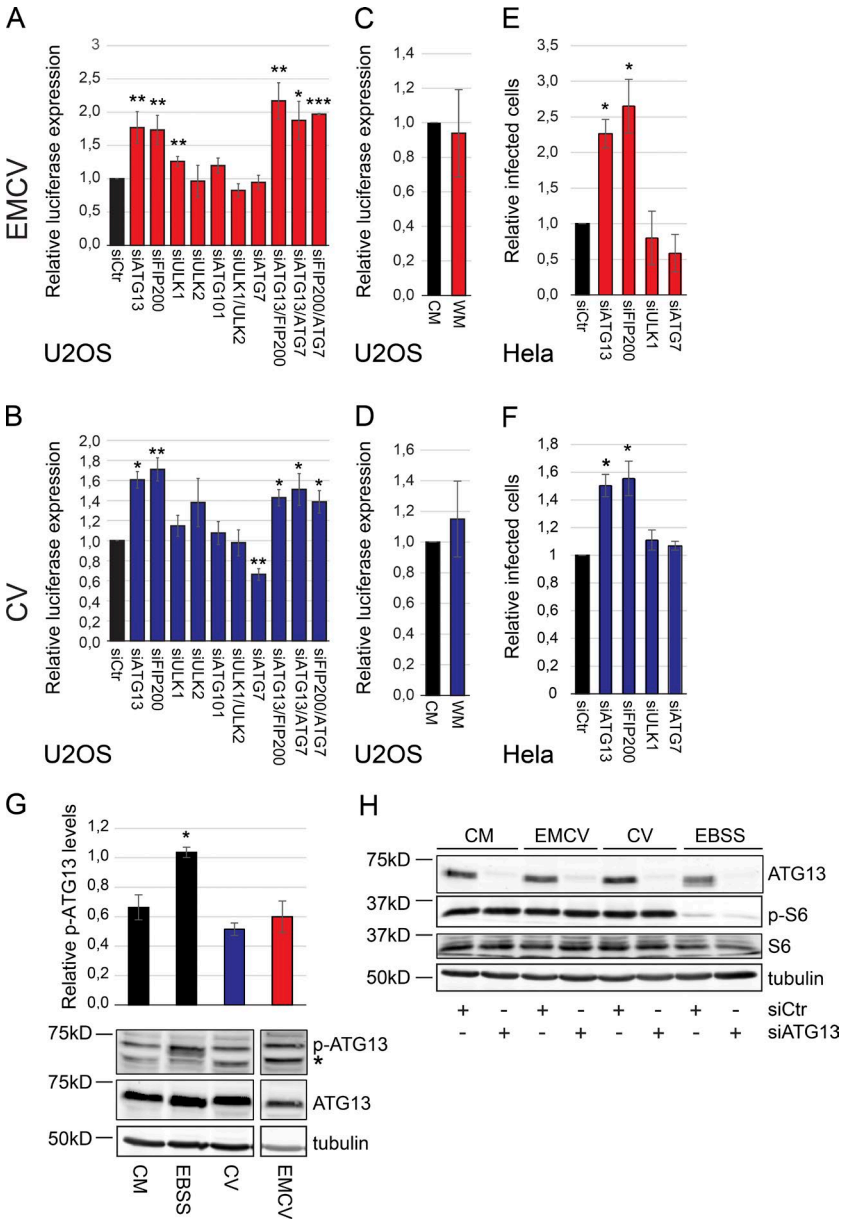

Figure 4. **ATG13 and FIP200 control EMCV and CV replication independently of their autophagic function as part of the ULK complex.** (A and B) The indicated *ATG* genes were depleted in U2OS cells before infecting cells with luciferase-expressing EMCV (A) or CV (B) and measuring luciferase expression (A, n = 4; B, n = 3). (C and D) U2OS cells were infected with luciferase-expressing EMCV (C) or CV (D) in the presence or absence of 233 nM wortmannin (WM) before assessing luciferase expression (n = 3). (E and F) The indicated *ATG* genes were depleted HeLa cells before infected with EMCV (E) or CV (F). Cells were stained using antibodies against viral proteins and the number of infected cells was determined by automated quantification of immunofluorescence images (n = 3). (G) U2OS cells were infected or not with EMCV or CV, or they were nutrient-starved (EBSS). ATG13 and phosphorylation of ATG13 on serine 318 (p-ATG13) levels were determined and quantified by Western blot (n = 4). Asterisk indicates a cross-reacting band. (H) U2OS cells depleted or not of ATG13 were infected or not with EMCV or CV, or they were nutrient starved. Levels of ATG13, the S6 protein, and the S6 protein phosphorylated in serines 235 and 236 (p-S6) were analyzed by Western blot. All data are presented relative to the control (folds). Error bars represent SEM. *, $P < 0.05$; **, $P < 0.01$; ***, $P < 0.001$; no symbol indicates not significant. CM, control medium; siCtr, scramble siRNA.

of the EV-C species; Tebruegge and Curtis, 2009), or a mutant EMCV called EMCV-Zn that is unable to suppress innate antiviral responses such as the type I IFN (IFN-α/β) response in the host cells (Hato et al., 2007; Langereis et al., 2013; Fig. 9). Depletion of FIP200 and ATG13 reduced the percentage of surviving cells infected by the three tested viruses (Fig. 9 A). The decrease in cell survival upon ATG13 and FIP200 depletion was always accompanied by an increase in virus progeny (Fig. 9 B), which was not observed upon ATG7 depletion. These results strongly indicate that ATG13 and FIP200 play an important role in controlling the vast majority of picornaviral infections independently of their role in autophagy.

ATG13 and FIP200 regulate picornaviral replication through a mechanism that does not directly interfere with viral components or the type-I IFN response

A possible mechanism how ATG13 and FIP200 might influence virus replication could be through the IFN-α/β response pathway regulation. Therefore, we tested the mRNA transcription levels of TNF-α, IFN-β< and CXCL10 upon knockdown of either ATG13, FIP200, or ATG7 (Fig. S4, C–E). We did not observe a significant change in TNF-α and IFN-β mRNA levels (Fig. S4, C and D), whereas CXCL10 mRNA levels were elevated upon ATG13, FIP200, and ATG7 depletion (Fig. S4 E), indicating that autophagy is important for its regulation, as previously documented (Kaizuka and Mizushima, 2015).

To gain more insight into the potential process through which ATG13 and FIP200 control picornaviral infections, we explored by protein mass spectrometry (MS) whether ATG13 and FIP200 bind viral factors or eventually different proteins when cells are exposed to CV infection. To this aim, we induced HA-ATG13 or HA-FIP200 expression in HEK293T-REx cells with doxycycline for 24 h and infected them with CV for 6 h or left them uninfected. HEK293T-REx cells not carrying a construct served as a control. Cells were subjected to HA immunoprecipitations and analyzed by liquid chromatography/tandem MS (Suzuki et al., 2015a; see Table S6 for complete

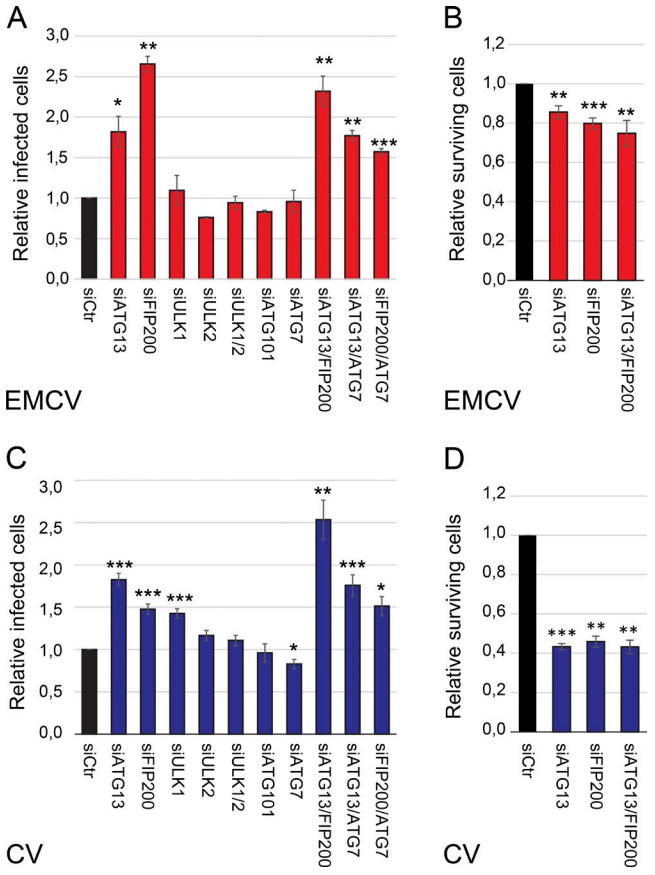

Figure 5. **ATG13 and FIP200 act in the same pathway that controls EMCV and CV replication.** (A and C) The indicated genes were knocked down in U2OS cells before inoculating EMCV (A) or CV (C) for 6 h and determining the number of infected cells (n = 3). (B and D) The number of surviving cells was determined after infection with EMCV for 24 h (B) or CV for 48 h (D; n = 3). All data are presented relative to the control (folds). Error bars represent SEM. *, P < 0.05; **, P < 0.01; ***, P < 0.001; no symbol indicates not significant. siCtr, scramble siRNA.

proteomic data). As expected, ATG13 and FIP200 were binding the other subunits of the ULK complex (Behrends et al., 2010) in infected and uninfected cells, as well as known interactors such as ATG9A (Suzuki et al., 2015b) and components of the C9orf72–SMCR8–WDR41 complex recently found to regulate autophagy (Sullivan et al., 2016; Fig. S4 F). Importantly, we did not find an interaction between either ATG13 or FIP200 with any of the CV proteins, or main changes in the interactome of ATG13 and FIP200, upon infection (Fig. S4 F and Table S6). In addition, a distribution analysis of ATG13 and FIP200 during CV and EMCV infection in U2OS cells by immunofluorescence showed no colocalization between these two proteins with the viral replication complexes (unpublished data). Furthermore, depletion of ATG13, FIP200, or ATG7 did not change the localization of either EMCV or CV replication complexes compared with the control cells (Fig. S5, A–D). We also did not observe differences in the morphology of the CV replication structures upon ATG13 depletion compared with the control by electron microscopy (Fig. S5, F and G). This type of analysis, however, showed that there are more cells displaying typical CV replication structures, which appear late in CV life cycle (Fig. S5 E, category 1; Limpens et al., 2011), confirming the finding that ATG13 depletion accelerates the infection by this virus (Fig. S5 E). Altogether, these results strongly suggest that ATG13 and FIP200 regulate picornavirus replication through a process that does not directly interfere with viral components.

RNA sequencing highlights potential ATG13 and FIP200 unconventional functions in picornaviral infection control

To gain insights into the potential cellular processes that are specifically regulated by ATG13 and FIP200 and could be relevant to control picornaviral infections, we performed RNA sequencing to compare mRNA expression profiles in U2OS cells depleted of ATG13, FIP200, or ATG7 or control cells exposed or not to CV infection (Fig. 10; see Table S7 for complete RNA sequencing data). To identify genes and pathways that are differentially regulated in ATG13 and FIP200 knockdown cells, but not in those depleted of ATG7, we extracted the genes that were differentially expressed in ATG13- and FIP200-depleted cells compared with control cells and furthermore did not display expression changes in the absence of ATG7. We categorized these genes as up-regulated and down-regulated, separating uninfected and CV-infected cells (Fig. 10 A). The RNA-sequencing analysis revealed, in uninfected cells, that 83 genes were up-regulated and 142 down-regulated by ATG13 and FIP200 depletion in an autophagy-independent manner. In CV-infected cells, we identified 32 up-regulated and 36 down-regulated genes (Fig. 10 A). Most of the identified genes are involved in transcriptional regulation, transport, apoptosis, cell cycle regulation, and ubiquitin conjugation (Fig. 10 B). Accordingly, Gene Ontology analysis showed that most of the genes localized to the nucleus and the cytoplasm, but others also localized to endomembranes such as the ER and mitochondria. In line with our data (Figs. S4 and S5), we did not observe an enrichment of genes involved in the antiviral IFN-α/β response in CV-infected cells. Collectively, our RNA-sequencing results point to several processes involving ATG13 and FIP200 outside the context of autophagy, and one or more of them might play a role controlling picornavirus infection.

Discussion

Autophagy is an important cell survival mechanism that contributes to the maintenance of cellular homeostasis in physiological and pathological conditions (Meijer and Codogno, 2004). To investigate the contribution and relevance of this process in specific situations, one of the most frequently used approaches has been and still is the depletion of ATG proteins. Large parts of the studies rely on the ablation of only one ATG protein, which is sufficient to inhibit autophagy. An emerging number of studies, however, are revealing that ATG proteins have also functions that are not related to their role in autophagy (Bestebroer et al., 2013; Subramani and Malhotra, 2013). As a result, it could be that some of the processes that have been associated with autophagy are not linked with this pathway but simply connected with one or more of these unconventional functions of the ATG proteins, as recently shown for neutrophil-mediated immunopathology during *Mycobacterium tuberculosis* infection. Here, ATG5 has a unique autophagy-independent role in protection against the pathogen and not as previously assumed as partof the autophagy machinery (Kimmey et al., 2015). Similarly, ATG12 has a potentially distinct function from autophagy in pro-opiomelanocortin–expressing neurons because,

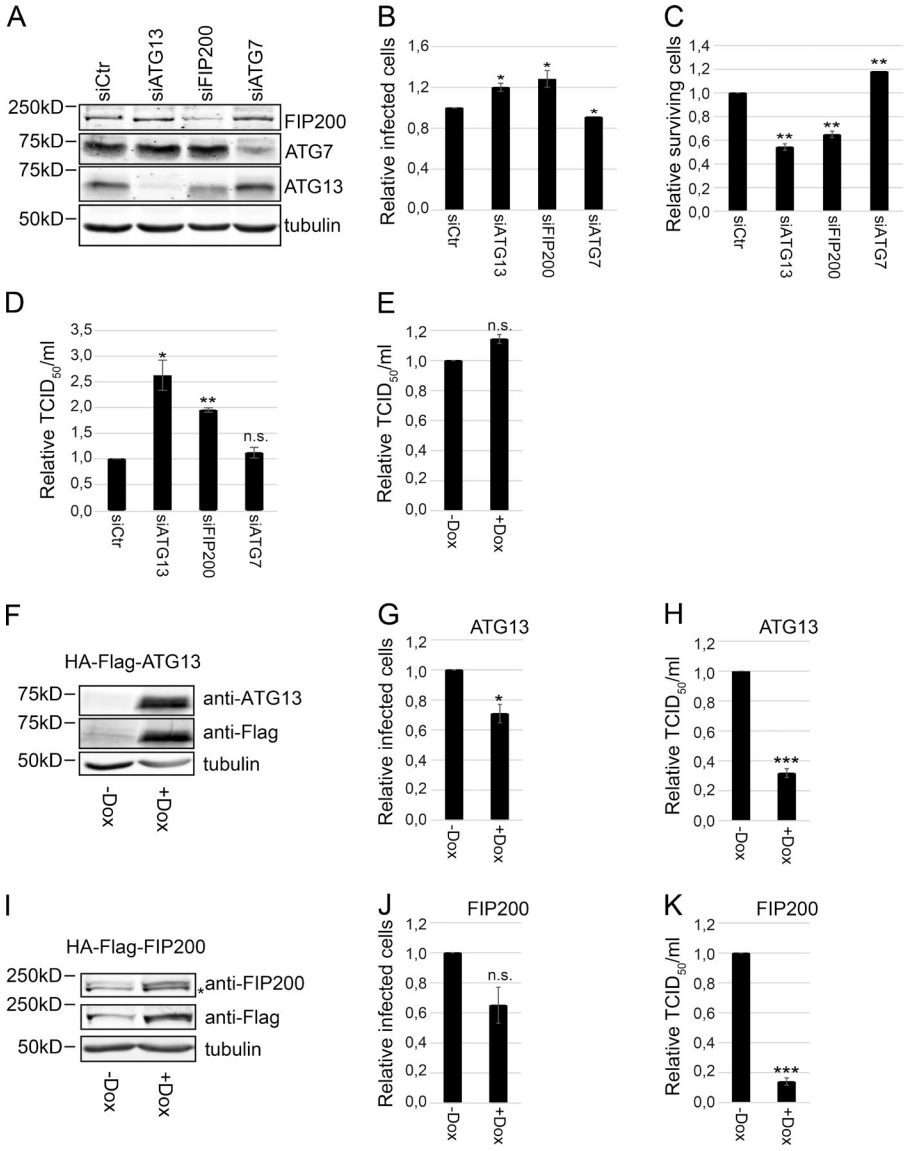

Figure 6. **Viral replication of CV is reduced upon expression of ATG13 or FIP200 in HEK293T cells.** HEK293T-REx cells were transfected with siRNA targeting ATG13, FIP200, or ATG7 or scramble siRNA (siCtr) for 48 h. (A) Protein knockdown in HEK293T-REx cells was determined by Western blot. (B) Cells transfected as in A were exposed to CV at an MOI of 0.5 before quantifying the number of infected cells after 6 h (n = 4). (C and D) Cells transfected as in A were infected with CV at an MOI of 0.02, and after 24 h, the number of surviving cells (C) and the virus titer in the supernatant (D) were determined (n = 3). (E) HEK293T-REx cells were treated with doxycycline (Dox) for 24 h, and CV titer was determined. (F–K) HEK293T-REx-HA-Flag-ATG13 (F–H) or HEK293T-REx-HA-Flag-FIP200 (I–K) cells were treated for 24 h with doxycycline to induce protein expression or left untreated before to be exposed to CV at MOI 0.5. The protein expression was analyzed by Western blot before virus inoculum (F and I). The number of infected cells was quantified upon 6 h (G and J; n = 4), whereas the CV titer was determined after 24 h (H and K; n = 3). All data are presented relative to the control (folds). Error bars represent SEM. *, P < 0.05; **, P < 0.01; ***, P < 0.001; n.s., not significant. siCtr, scramble siRNA.

in contrast to that of ATG5, its specific deletion in these cells causes an acceleration in weight gain upon a high-fat diet and disrupts the energy balance in mice (Malhotra et al., 2015). These studies clearly show that key ATG genes such as ATG5 and ATG12 fulfill unconventional functions beyond autophagy. Furthermore, there are also unconventional functions of ATG proteins in the complexes involved in autophagy initiation such as ULK1/2, which, for example, functions in ER-to-Golgi trafficking (Joo et al., 2016).

To estimate the chance of investigating an unconventional function when knocking down a single ATG protein, we have conducted, to the best of our knowledge, the first screen that simultaneously address the role of the entire ATG proteome. Our screen also took into account documented and possible functional redundancies between proteins. By monitoring the replication of viruses from six different virus families, our goal was to determine in how many of these situations autophagy or an unconventional role of ATG proteins was positively or negatively involved by supporting or inhibiting viral replication. We performed our screen in two different cell lines to exclude cell line–specific functions. The importance of this approach is reflected by the results we obtained with VaV and SFV. We observed clear opposite effects on VaV and SFV replication upon ATG proteome depletion depending on the cell line. This result could explain some of the discrepancies in the literature, such as the one for EMCV in which depletion of autophagy genes in different cell lines was either beneficial or unfavorable for the virus (Zhang et al., 2011; Chakrabarti et al., 2012).

Overall, our screen reveals that autophagy is not positively or negatively involved in the replication of any of the tested viruses, even if we have observed a tendency for this pathway to be important for optimal HSV-1 replication, as has been suggested for two other members of the alphaherpesviruses, i.e., HSV-2 and varicella-zoster virus (Buckingham et al., 2015; Yakoub and Shukla, 2015). In contrast, we have found that 16 out of 44 tested ATG proteins (36%) might have unconventional functions, and this number increases to 20 out of 44 ATG proteins (45%) if we also include those ATG proteins that are exclusively found to be relevant for HSV-1 replication. Some of those 20 ATG proteins inhibit or support viral replication of more than one tested virus. In total, from the 360 different combinations that we tested, we identified 14 hits that inhibit viral replication and 21 hits that support viral replication. In agreement with the literature, UVRAG was among the proteins that

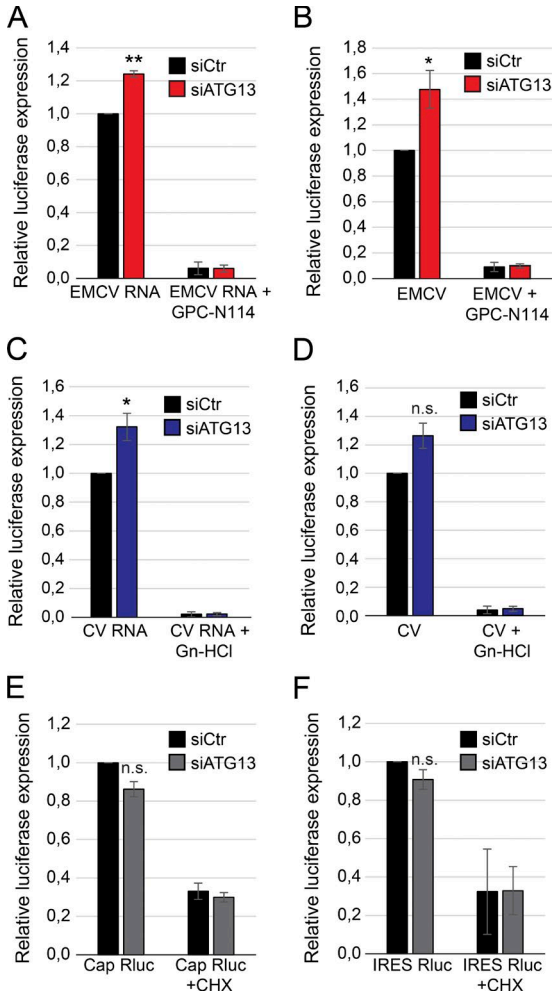

Figure 7. **ATG13 depletion enhances EMCV and CV replication, but not virus cell entry.** (A) U2OS cells depleted or not of ATG13 using siRNA for 48 h were transfected with Renilla luciferase EMCV RNA for 7 h. GPC-N114 was added or not 1 h after virus inoculation before measuring luciferase expression (n = 3). (B) Cells prepared as in A were infected with luciferase-expressing EMCV for 7 h. GPC-N114 was added or not 1 h after virus inoculation before assessing luciferase expression (n = 5). (C) Cells prepared as in A were transfected with Renilla luciferase CV RNA for 7 h. Guanidine-HCL (Gn-HCl) was added or not 1 h posttransfection before measuring luciferase expression (n = 4). (D) Cells prepared as in A were infected with luciferase expressing CV for 7 h. Gn-HCl was added or not 1 h after virus inoculation before assessing luciferase expression (n = 4). (E) Cells were transfected with the cap RNA Renilla-luciferase (Rluc) transcript for 7 h and, when indicated, cycloheximide (CHX) was added 1 h after transfection before determining luciferase expression (n = 3). (F) Cells were transfected with the IRES-luciferase RNA transcript for 7 h and when indicated, CHX was added 1 h after transfection before measuring luciferase expression. (n = 3). All data are presented relative to the control (folds). Error bars represent SEM. *, $P < 0.05$; **, $P < 0.01$; n.s., not significant. siCtr, scramble siRNA.

we found to be necessary for IAV infection (Pirooz et al., 2014). We also confirmed that neither ATG7 (Reggiori et al., 2010) nor ATG5 (Zhao et al., 2007) is required for MHV replication, and in agreement with the literature, we observed a tendency for MHV replication to be dependent on the LC3 proteins (Reggiori et al., 2010). Very little is known about the involvement of autophagy in the SFV and VaV life cycles. Although it seems that, upon SFV infection, there is an accumulation of autophagosomes caused by a block in this pathway, the virus titer is unchanged in *ATG5*$^{-/-}$ MEFs (Eng et al., 2012). VaV appears to block autophagosome formation upon infection, but in this case, the virus titer is unaffected in *ATG3*$^{-/-}$ and *ATG5*$^{-/-}$ MEFs or *BECLIN1*$^{-/-}$ embryonic stem cells (Zhang et al., 2006; Moloughney et al., 2011). The results of our screen are consistent with these observations, but they also point to a tissue-specific interplay between SFV/VaV and autophagy. Although we could confirm data from the literature with this screen, we cannot exclude that the results in physiologically relevant target cells or in in vivo models might be different from the ones in the immortalized cell lines that we used.

To validate our screening approach and identify unconventional functions of ATG proteins, we focused on ATG13, because its depletion markedly enhanced EMCV replication, whereas knockdown of other ULK complex components (such as ULK1, ULK2, or ATG101) did not. A detailed analysis confirmed that not only ATG13 but also FIP200 decrease EMCV replication independently of their function in autophagy (Fig. 10 C). Although FIP200 was not among the significant hits in the screen, EMCV replication was strongly up-regulated upon its depletion. In contrast to what was found for UVRAG during IAV infection (Pirooz et al., 2014), ATG13 and FIP200, possibly in complex, control not virus cell entry but rather virus replication. Interestingly, the unconventional function of ATG13 and FIP200 is not restricted to EMCV but also controls more members of the picornavirus family, i.e., CVB3, CVA21, and EV71. It has been shown that picornaviruses induce autophagy upon infection, and this is beneficial for both enterovirus 71 (Huang et al., 2009; Lee et al., 2014; Fu et al., 2015) and CV (Wong et al., 2008; Kemball et al., 2010; Alirezaei et al., 2012, 2015; Tabor-Godwin et al., 2012), whereas it is still a matter of debate whether autophagy has also a proviral role for EMCV (Zhang et al., 2011; Chakrabarti et al., 2012). Based on the conclusions of these studies, one would expect that depletion of any ATG protein that blocks autophagy should inhibit the picornavirus life cycle as well. Although we blocked autophagy by ATG13 and FIP200 depletion, we did not observe impairment in picornaviral life cycles. On the contrary, viral replication and subsequent viral particle production were strongly enhanced in the absence of these two proteins, even in cells where ATG7 was simultaneously depleted. It has previously been indicated that autophagy is essential for picornavirus infections mostly through the use of pharmacological autophagy inhibitors but also through BECLIN1, VPS34, LC3, and ATG7 knockdown (Wong et al., 2008; Zhang et al., 2011; Delorme-Axford et al., 2014). Pharmacological inhibitors or BECLIN1 and VPS34 depletion affects specific endosomal functions, and this could also have an impact on picornaviral infections, depending on the cell type. We confirmed, to a certain extent, the inhibitory effect of ATG7 knockdown (Figs. 4, 5, 7, and 8), which would suggest that this protein, like ATG13 and FIP200, influences picornavirus infection through an unconventional role in a different pathway. Alternatively, the fact that picornaviruses can exploit more than one pathway for replication, including autophagy (Alirezaei et al., 2015), could explain the relevance of ATG proteins in specific cell types, as was shown for pancreatic acinar cells, in which ATG5 deletion reduces CV replication as well as pathogenesis (Alirezaei et al., 2012).

The notion that ATG13 and FIP200 have important autophagy-independent functions is underlined by the fact that although most autophagy-deficient mice, including *ULK1*$^{-/-}$ *ULK2*$^{-/-}$ animals (Joo et al., 2016), die shortly after birth,

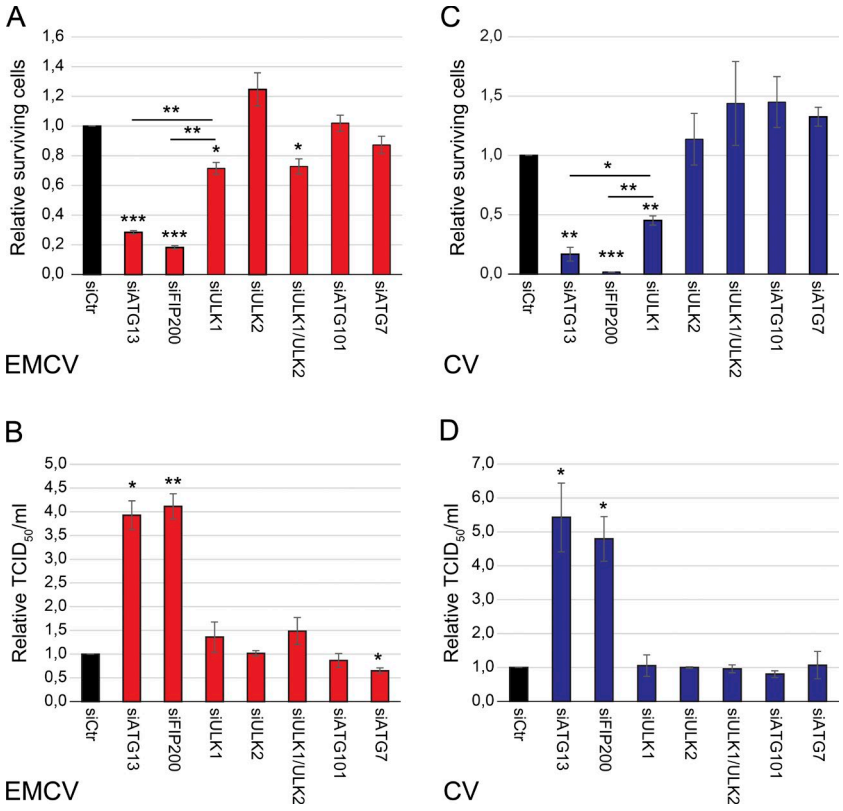

Figure 8. **Depletion of ATG13 and FIP200 results in higher EMCV and CV production in host cells.** (A) The indicated genes were depleted of U2OS cells for 48 h using siRNA before infecting cells with EMCV at an MOI of 0.1 for 24 h and subsequently determining the number of surviving cells (n = 3). (B) The culture supernatants of the experiment in A were collected, and the virus titer was measured using the $TCID_{50}$ assay (n = 3). (C) Cells prepared as in A were infected with CV at an MOI of 0.01 for 48 h before determining the number of surviving cells (n = 3). (D) The culture supernatants of the experiment in C were collected, and virus titer was measured using the $TCID_{50}$ assay (n = 3). All data are presented relative to the control (folds). Error bars represent SEM. *, P < 0.05; **, P < 0.01; ***, P < 0.001; no symbol indicates not significant. siCtr, scramble siRNA.

FIP200$^{-/-}$ and *ATG13*$^{-/-}$ mice die during embryonic development (Joo et al., 2011; Hieke et al., 2015; Kaizuka and Mizushima, 2015). Our RNA-sequencing analysis supports this observation, as a subset of the genes that we found to be differentially expressed in absence of ATG13 and FIP200 are involved in transcriptional regulation and development (11 out of 225 in uninfected cells and 8 out of 68 in infected cells). These results are in line with the requirement of ATG13 and FIP200 in embryonic development in an autophagy-independent manner (Chen et al., 2016). A possible link how ATG13 and FIP200 regulate this developmental process could be HSBP1, which we identified as a new interactor of ATG13 and FIP200 (Fig. S4), and which is also required for embryonic development (Eroglu et al., 2014).

Other scenarios could also explain how ATG13 and FIP200 deficiency increases picornavirus replication. A large subset of differentially regulated genes in ATG13- and FIP200-depleted cells (102 out of 293) code for integral or membrane-associated

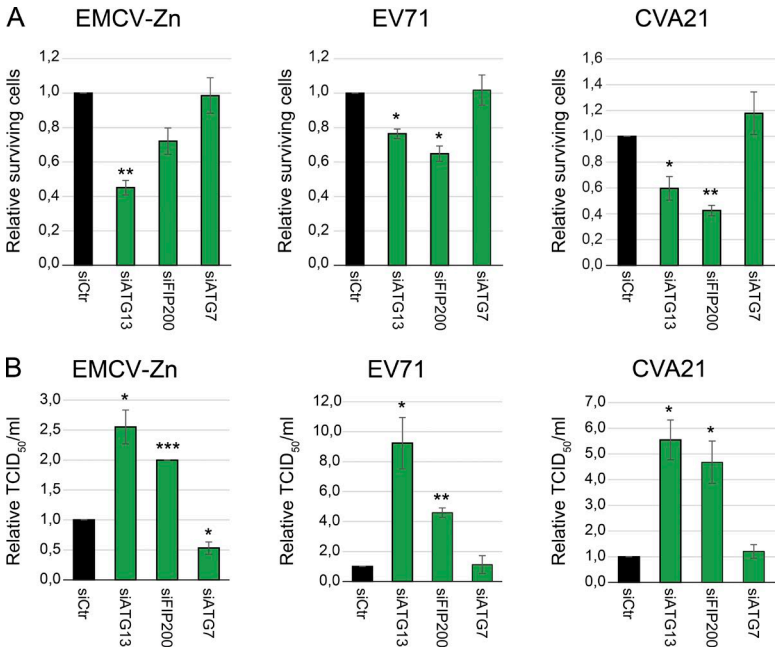

Figure 9. **Depletion of ATG13 and FIP200 results in higher picornavirus production in host cells.** (A) Cells were transfected with siRNA against ATG13, FIP200, ATG7, or scramble siRNA (siCtr) for 48 h, and the number of surviving cells was determined after 24 h of infection with EMCV-Zn (in U2OS cells), EV71 (in U2OS cells), or CVA21 (in HeLa cells) at MOI 0.1 (n = 3). (B) The culture supernatants of the experiment in A were collected, and the virus titer was measured using the $TCID_{50}$ assay (n = 3). Error bars represent SEM. *, P < 0.05; **, P < 0.01; ***, P < 0.001; no symbol indicates not significant. siCtr, scramble siRNA.

A

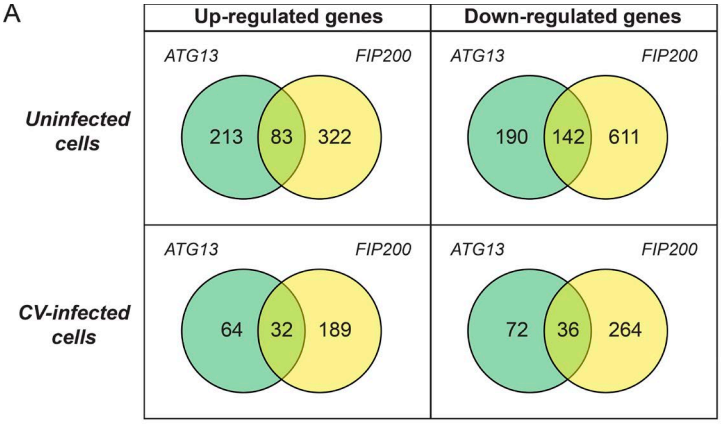

B

Biological process

	Transcriptional regulation	Transport	Apoptosis	Cell cycle	Ubl conjugation pathway
uninfected	31	27	20	16	12
CV infected	8	3	-	2	3

Cellular component

	Nucleus	Membrane	Cytoplasm	ER	Mitochondria
uninfected	83	82	69	25	22
CV infected	25	20	16	7	5

C

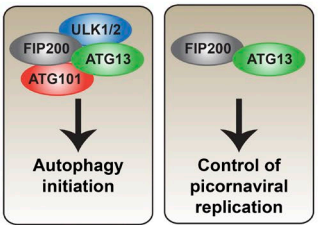

Figure 10. **RNA sequencing provides insight into the unconventional function(s) of ATG13 and FIP200.** U2OS cells depleted of ATG13, ATG7, or FIP200, or treated with control siRNA, were infected or not with CV for 7 h at MOI 1. RNA sequencing was performed on isolated RNA as described in Materials and methods. (A) Venn diagrams showing up- and down-regulated genes in ATG13- and FIP200-depleted cells, whose expression was not altered in ATG7 knockdown cells. The overlapping areas indicate genes that are differentially expressed in both ATG13- and FIP200-depleted cells. Genes whose transcription is also altered in ATG7-depleted cells were not considered, because their differential expression is very likely linked to one or more functions of autophagy. (B) Gene Ontology analysis of the genes that were differentially and specifically expressed in ATG13- and FIP200-depleted cells, exposed or not to CV. (C) Schematic model for the autophagy-dependent and -independent functions of ATG13 and FIP200.

proteins, and although we did not observe major differences in viral replication structures in ATG13 knockdown cells, these proteins could still participate in the optimal establishment of picornaviral replication structures. Because ATG13 has been implicated in selective forms of autophagy in mammalian cells and plants (Joo et al., 2011; Li et al., 2014), there is also the possibility that ATG13 and eventually FIP200 function in one of these pathways to prevent picornavirus replication. The exact mechanism by which ATG13 and FIP200 affects picornavirus genomic RNA replication remains to be established. Therefore, the RNA-sequencing and MS datasets that we generated in this study are valuable tools for future studies aimed at unraveling the precise unconventional cellular function of ATG13 and FIP200.

The proof-of-principle study on FIP200 and ATG13 validated our ATG-specific siRNA screening approach as a platform to identify unconventional roles of ATG proteins. The screen thus strongly supports the emerging concept that ATG proteins do not participate exclusively in autophagy. It also calls for caution in interpreting results on the contribution of autophagy to a specific process that relies solely on the depletion of a single ATG protein.

Materials and methods

Antibodies and reagents

The following primary antibodies were used: rabbit anti-LC3 (Novus Biologicals), mouse anti-Flag (Sigma-Aldrich), mouse anti-tubulin (Sigma-Aldrich), rabbit anti-ATG13 (Sigma-Aldrich), rabbit anti-ULK1 (Santa Cruz Biotechnology, Inc.), rabbit anti-FIP200 (Bethyl Laboratories, Inc.), guinea pig anti-p62 (Progen), rabbit anti–phospho-ATG13 (S318; Rockland), mouse antienterovirus (Dako), rabbit anti-CV2bc (a gift from L. Whitton, Scripps Research Institute, La Jolla, CA), rabbit anti-Capsid (EMCV; a gift of A. Palmenberg, University of Wisconsin, Madison, WI), mouse anti-dsRNA (English & Scientific Consulting Bt.), and rabbit anti-ATG7 (Cell Signaling Technology). Goat anti–mouse and chicken anti–rabbit Alexa Fluor 488–conjugated antibodies, goat anti–mouse and donkey anti–rabbit Alexa Fluor 568–conjugated antibodies, goat anti–mouse antibodies, goat anti–rabbit Alexa Fluor 680–conjugated antibodies, and goat anti–mouse and goat anti–rabbit Alexa Fluor 800–conjugated antibodies were used for the visualization of the primary antibodies. All secondary antibodies and DAPI were from Invitrogen and Thermo Fisher Scientific. Puromycin, guanidine hydrochloride, and cycloheximide were purchased from Sigma-Aldrich, blasticidin was purchased from Invivogen, and doxycycline was purchased from Takara Bio, Inc. GPC-N114 is a nonnucleoside inhibitor that targets the enterovirus RNA-dependent RNA polymerase and exerts broad-spectrum antiviral activity against all enteroviruses (van der Linden et al., 2015).

Cell lines and cell culture

U2OS (a gift from G. Strous, University Medical Center Utrecht, Utrecht, Netherlands), HeLa-mCeaCam1, HEK-mCeaCam1 (Wicht et al., 2014), HEK293T-REx, HA-Flag-ATG13 and HA-Flag-FIP200 (Behrends et al., 2010; Jung et al., 2015), BGM kidney, baby hamster kidney 21 (BHK-21) and HeLa cells, and immortalized *ATG13*$^{-/-}$ mouse embryonic fibroblasts (MEFs; a gift from X. Wang, National Institute of Biological Science, Beijing, China) retrovirally transformed

with an empty vector or with a plasmid carrying HA-ATG13 (Hieke et al., 2015), were cultured in DMEM (Thermo Fisher Scientific) supplemented with 100 U/ml penicillin, 100 µg/ml streptomycin, and 10% FCS at 37°C in 5% CO_2 humidified atmosphere. 4 µg/ml blasticidin and 2 µg/ml puromycin were added for culturing the HEK293T-REx cells expressing HA-Flag-ATG13 or HA-Flag-FIP200 (Behrends et al., 2010; Jung et al., 2015). HeLa-mCeaCam1 and HEK-mCeaCam1 were generated by transducing the cells with mCeaCam1 (murine carcinoembryonic antigen-related cell adhesion molecule 1a) using a Moloney murine leukemia virus packaging vector (Wicht et al., 2014). Stable cell lines were made using G418 selection. HEK293T-REx, HA-Flag-ATG13, and HA-Flag-FIP200 were generated by retroviral transduction of the according MSCV-i(N-Flag-HA)-IRES-PURO constructs (Behrends et al., 2010; Jung et al., 2015).

To induce autophagy, cells were washed two times with Earle's balanced salt solution (EBSS; Sigma-Aldrich) and then incubated in the same medium for 2 h.

Virus stocks

Virus stocks were generated and propagated as described previously. Fluc-HSV-1 (Paludan virus stock collection), SFV-Rluc was produced from the infectious clone SFV-RlucH2 and propagated in BHK cells (Pohjala et al., 2011), MHV-2aFLS was propagated on LR7 mouse fibroblast cells (de Haan et al., 2003), Fluc-VaV was propagated in African green monkey kidney BSC-40 cells (Rodriguez et al., 1988; de Vries et al., 2011), and IAV-WSN luciferase pseudovirus was produced in a MDCK cell line that stably expresses the HA of IAV-WSN (König et al., 2010; de Vries et al., 2011). EMCV, EMCV-Zn wild type (Hato et al., 2007), and Rluc-EMCV (Lanke et al., 2009) were generated by transfecting runoff transcript RNA from the BamHI linearized pM16.1 infectious clone into BHK21 cells. The CVB3 and RLuc-CVB3 (Wessels et al., 2005) viruses were generated by transfecting runoff transcript RNA from the SalI linearized p53CVB3/T7 infectious clone into BGM cells. CVB3, EV68 (Ulferts et al., 2013), EV-71, and CVA21 (van der Schaar et al., 2013) viruses were propagated in HeLa-R19 cells, whereas EMCV was propagated in BHK21 cells.

Virus infection

Virus infections were performed at an MOI of 0.2–2 in all the experiments except when determining the amount of surviving cells and the virus titer subsequently at 24 h and 48 h after infection. In these cases, cells were infected at an MOI of 0.01 for CV and 0.1 for all other viruses. The virus titers were determined using a tissue culture infectious dose assay according to the Reed–Muench method (Reed and Muench, 1938).

siRNA-based screens

The customized ON-TARGETplus SMARTpool human siRNA library (Table S1) and the deconvoluted ON-TARGETplus SMARTpools were obtained from GE Healthcare. The screens were run in 96-well plates, and the rows of wells on the limits of the plates were not used to avoid change in the readout caused by a differential in cell growth. 2 pmol siRNA per well was used for single gene knockdown, whereas for multiple gene depletions, total amounts of 3 pmol (double knockdowns), 4.5 pmol (triple knockdowns), or 6 pmol (quadruple knockdowns) were used. Reverse transfection was conducted according to the manufacturer's protocol using 0.1 µl RNAiMax and 3,000 cells (U2OS, HeLa-mCC1 or HEK-mCC1 cells) per well in a final volume of 100 µl DMEM containing 100 U/ml penicillin, 100 µg/ml streptomycin, and 10% FCS. These conditions, which were set with pilot experiments, allowed optimal knockdown of the target genes without causing cell death (unpublished data). The customized siRNA library also included probes knocking down genes known to be relevant for the replication of one or more viruses. Runs of the screen where these positive controls gave no change in luciferase activity were discarded and repeated. The genes used for this purpose were GBF1 and ARF1 for MHV (Verheije et al., 2008), PI4KA for EMCV (Dorobantu et al., 2015), and ATP6V1A for IAV and SFV (Ochiai et al., 1995; Glomb-Reinmund and Kielian, 1998).

Typically, cells were processed in two ways after the siRNA-mediated knockdown for 48 h. For analyzing endogenous p62 and LC3 puncta accumulation in order to measure autophagy, cells were fixed with 4% PFA and then incubated with the blocking buffer (PBS, 1% bovine serum albumin, and 0.1% saponin) before being stained first with p62 and LC3 antibody and then with Alexa Fluor 568– and 488–conjugated secondary antibodies. Nuclei were stained with Hoechst 33342 (Sigma-Aldrich) during incubation with the secondary antibody. To examine virus replication, 50 µl of culture medium was aspired and replaced with 50 µl fresh culture medium containing virus strains carrying the luciferase gene at an MOI of 0.2. Infections were conducted for 6 h for EMCV, VaV, HSV-1, SFV, and MHV and 16 h for IAV before lysing the cells and enzymatically measuring luciferase expression. The virus infection and LC3 puncta assessment screens were run four times, whereas the ones for p62 puncta quantification were run three times.

Luciferase assays

Cells in 96-well plates were washed with PBS and incubated with 50 µl lysis buffer (Thermo Fisher Scientific) at room temperature for 15 min before storing the cell lysates at −20°C. 25-µl aliquots of thawed cell lysate were then used to measure either Firefly or Renilla luciferase expression (depending on the gene carried by the assayed virus) using either the Firefly or Renilla luciferase flash assay kit (both from Thermo Fisher Scientific). Alternatively, Renilla luciferase activity was measured in the following reaction buffer: 45 mM EDTA, 30 mM sodium pyrophosphate, 1.425 M NaCl, and 10 µM coelenterazine h (Promega; Baker and Boyce, 2014).

Enzymatic activities were measured using a GloMax-Multi Detection System (Promega) and the following program: 25 µl substrate, 2 s delay, and 10 s measuring. Background luminescence was subtracted from each obtained value, and the results were always normalized toward cells transfected with control siRNA.

Analysis of the screen data

Raw luciferase measurements from four independent experiments were standardized creating a Z-score. The distance of the Z-score from each siRNA pool to the control siRNA was determined from the four independent experiments. The median Z-score and the SD of the mean were then determined (Table S5). Z-score values below −1.96 and above 1.96 were considered as statistically significant. Data were finally expressed in an x–y graph, where the x axis projects the results obtained in the screen in the U2OS cells or HEK cells for MHV and the y axis projects those acquired in HeLa cells.

Western blot analyses

Cells grown in six-well plates were washed with PBS and harvested in 100 µl lysis buffer (TBS, 1% Triton-X100, and protease inhibitors) or lysed in an alternative lysis buffer (1% Triton X-100, 150 mM NaCl, 1 mM EDTA, 0.5% sodium deoxycholate, 0.1% SDS, 50 mM Tris-HCl, pH 8.0, protease inhibitors, and 5 mM sodium fluoride) for detection of phospho-ATG13. The lysates were incubated on ice for 30 min, vortexed, and centrifuged at 14,000 *g* for 10 min at 4°C. The supernatants were collected and mixed with Laemmli loading buffer (Laemmli, 1970). Equal protein amounts were separated by SDS-PAGE, and after standard Western blotting, proteins were detected using specific antibodies

and the Odyssey Imaging System (LI-COR Biosciences). Protein signal intensities (densitometric values) were normalized against a tubulin loading control for each sample. Densitometric values were determined and quantified on Western blots at nonsaturating exposures using the ImageJ software (Schneider et al., 2012).

Long-lived protein degradation assay

The protocol is identical to the one already described, with few modifications (Chan et al., 2007). U2OS cells grown in six-well plates were transfected for 48 h with control siRNA or siRNA targeting ATG13, ULK1, or FIP200. Subsequently, the medium was exchanged with the labeling medium (DMEM and 10% dialyzed FCS containing 0.2 µCi/ml [^{14}C]-valine + 65 µM valine). After 18 h, the cells were placed into chase medium (DMEM, 10% FCS, and 2 mM valine) and incubated for additional 4 h to allow degradation of short-lived proteins. Cells were then transferred for 2 h in the EBSS medium to induce autophagy or in DMEM containing 10% FCS (no autophagy stimulation). The culture media were collected, and TCA was added to 10%. After centrifugation at 2,000 rpm for 10 min, the radioactivity in the soluble fraction (SF) was measured by scintillation counting. In parallel, cells were lysed in PBS containing 1% Triton-X and TCA was added to the lysate to 10% before freezing the samples overnight at −20°C. The radioactivity of TCA-soluble fraction (cytosol) as well as that of the TCA-insoluble pellet (pellet) dissolved in Solvable solution (PerkinElmer) was then measured after centrifugation at 2,000 rpm for 10 min. Protein degradation was determined as follows: (counts in SF + counts in cytosol)/(counts in SF + counts in cytosol + counts in pellet).

siRNA and RNA transfections

After deconvolution, individual siRNAs were used for further experiments (Table S4). U2OS cells were transfected for 48 h with 20 nM of control siRNA or of siRNA targeting ATG13, ATG7, ATG101, ULK1, ULK2, or FIP200 (all from GE Healthcare) using 0.1 µl or 2 µl Lipofectamine RNAiMAX (Invitrogen) for 96- or 6-well plate cultures, respectively, according to the manufacturer's protocol. Combinations of two different siRNA probes were performed at total concentrations of 40 nM and 40 nM of control siRNA were used for these experiments. 10 ng CVB3 and EMCV Renilla luciferase RNA or 2 ng of Cap and IRES (Mengo) Renilla luciferase RNA was transfected into cells in 96-well plates using 0.1 µl of RNAiMax.

RNA isolation, cDNA synthesis, quantitative real-time PCR, and RNA sequencing

Total RNA was isolated from U2OS cells using an RNeasy mini kit (QIAGEN). Isolated RNA was either further processed for RNA sequencing or reverse transcribed into cDNA using a TaqMan reverse transcription reagents (Thermo Fisher Scientific). Real-time PCR was performed on a CFX96 Touch Real-Time PCR Detection System (Bio-Rad Laboratories) using the iQ SYBR Green Supermix kit (Bio-Rad Laboratories) and specific primers (Table S3). Alternatively, the Power SYBR Green Cells-to-CT kit (Thermo Fisher Scientific) was used according to manufacturer's protocol to isolate RNA, reverse transcribe the RNA, and synthesize cDNA. Quantitative PCR was performed in a CFX connect Thermocycler (Bio-Rad Laboratories) using specific primers (Table S3). RNA quality was controlled for integrity using capillary electrophoresis (Labchip GX; PerkinElmer) before RNA sequencing. Sample preparation was performed from 500 ng total RNA using the QuantSeq 3′ Library Prep kit (Lexogen), and 50-bp single-end samples were sequenced on an Illumina HiSeq2500. Gene expression quantification was performed as follows: The trimmed fastQ files were aligned to the human build b37 reference genome using hisat/0.1.5-β-goolf-1.7.20 (Kim et al., 2015) with default settings (stranded). Before gene quantification, SAMtools/1.2-goolf-1.7.20 (Li et al., 2009) was used to sort the aligned reads. The gene level quantification was performed by HTSeq-count HTSeq/0.6.1p1 (Anders et al., 2015) using mode = union. Ensembl version 75 was used as gene annotation database (Genome Analysis Facility of the University Groningen). Differentially expressed genes were identified using the DESeq2 package with standard settings (http://www.ncbi.nlm.nih.gov/pmc/articles/PMC4302049/). Genes with log2 fold change >0.2 and p adj <0.1 were considered as differentially expressed. All other genes were considered as unchanged in their expression compared with control cells. The UniProt website (http://www.uniprot.org/) was used for Gene Ontology and pathway analysis.

Immunoprecipitation and protein mass spectrometry

HA immunoprecipitation followed by mass spectrometric analysis was performed as previously described (Behrends et al., 2010). In brief, 293T-REx cells expressing HA-tagged proteins for 24 h were infected with CV for 7 h at an MOI of 2 or left uninfected before they were harvested and frozen at −80°C. Subsequently, cells were thawed and lysed with ice-cold MCLB buffer (50 mM Tris, pH 7.4, 150 mM NaCl, 0.5% NP-40, and complete EDTA-free protease inhibitor tablets; Roche), cleared through 0.45-µm spin filters (EMD Millipore), and immunoprecipitated using anti–HA-agarose (Sigma-Aldrich) overnight. After intensive washing, proteins were eluted with HA peptide (250 µg/ml; Sigma-Aldrich) and precipitated with TCA (Sigma-Aldrich), followed by digestion with trypsin (Promega) and desalting by custom-made stage tips. Samples were analyzed in technical duplicates on a LTQ Velos (Thermo Fisher Scientific), and spectra were identified as previously described (Huttlin et al., 2010). For CompPASS analysis, we used 142 unrelated bait proteins that were all previously processed in the same way (Sowa et al., 2009; Behrends et al., 2010). Weighted and normalized D-scores (WD^N-scores) were calculated based on average peptide spectral matches (APSMs). Proteins with $WD^N \geq 1$ and APSM ≥ 2 were considered as new interacting proteins.

Immunofluorescence and confocal microscopy

Cells were fixed with 4% PFA and washed and blocked with blocking buffer (PBS, 1% bovine serum albumin, and 0.1% saponin). Primary and secondary antibodies were diluted in the blocking buffer and incubated for 1 h. Nuclei were stained with Hoechst 33342 during the incubation with the secondary antibody for automated image acquisition. Alternatively, nuclei were stained with DAPI for confocal microscopy. Confocal microscopy was performed at room temperature using a laser-scanning microscope 700 (ZEISS) with a 63× 1.4 DIC Plan-Apochromat oil-immersion objective. ZEN digital imaging software (ZEISS) was used for image acquisition and processing of the images. All images were exported as TIFF images, and figures were finalized in Adobe Illustrator (Adobe).

Automated image acquisition

A Cellomics Arrayscan VTI HCS Reader (Thermo Fisher Scientific) was used to acquire cell images in the Hoechst, FITC and TRITC filters using either the 20×, 10×, or 5× lens for automated fluorescence signal acquisition.

A minimum of 400 cells per experiment was analyzed using the Cellomics SpotDetector V3 algorithm to determine the mean number of p62 and LC3 puncta per cell as well as the mean number of LC3 puncta area per cell. The Hoechst channel was used to set the autofocus; LC3 puncta were detected using the FITC filter, and p62 puncta were detected using the TRITC filter. An equal fixed exposure time was automatically set for all the samples, and LC3 and p62 puncta were detected in a cell area that excluded the nucleus. The numbers

of nuclei (valid object count), LC3 and p62 puncta per cell (spot per cell), and LC3 and p62 puncta area per cell (spot area per cell) were counted using this approach. To assess cell infection rate, cells were stained with either anti-capsid antibody when infected with EMCV or with anti-VP1 or anti-2bc antibodies, when infected with CV, before to image 5–30 fields of cells per sample using the Hoechst, FITC, or TRITC filters. The percentage of EMCV- or CV-positive cells was determined by analyzing the collected images using the cell counter application in ImageJ.

Cell death measurement

U2OS, HeLa or HEK293T-REx cells were infected at an MOI of 0.01 with CVB3 or an MOI of 0.1 with EMCV, EV71, EMCV-Zn, or CVA21 in DMEM for 2 h before replacing it with fresh DMEM supplemented with 100 U/ml penicillin, 100 µg/ml streptomycin, and 10% FCS and continuing the incubation for an additional 24–48 h. Supernatants were collected to determine the virus titer while cells were fixed with 3.7% PFA and cell nuclei were stained with Hoechst33342 and processed for automated image acquisition and analysis in the following way. The number of cells from four fields per well was determined by counting the number of nuclei using the Cellomics Arrayscan VTI HCS Reader with a 5× objective. The percentage of surviving cells in each sample was calculated by dividing the number of infected cells with that of uninfected cells.

Electron microscopy

U2OS cells were transfected with control siRNA or ATG13 siRNA for 48 h and infected with CV for 7 h at an MOI of 1. After a 2-h fixation at room temperature in 2% PFA and 2.5% glutaraldehyde in 0.1 M Na-cacodylate buffer, pH 7.4, cells were embedded in epon resin as previously described (Verheije et al., 2008). Subsequently, 70-nm sections were obtained using an UC7 Leica Ultra-microtome and stained with uranyl acetate and lead citrate as previously described (Verheije et al., 2008). Cell sections were analyzed using an 80-kV transmission electron microscope (CM100; FEI). Two independent grids were used to perform the counting analysis of 125 cells per condition in total. Three different categories of membranous rearrangements were identified in CV-infected cells and defined as follows: category 1, closely packed, elongated, regular shaped single-, double-, or multi-membrane vesicles; category 2, closely packed, irregular shaped, single-membrane vesicles with a light content; and category 3, irregular, collapsed membrane clusters.

Statistical analyses

Statistical significance was evaluated using two-tailed heteroscedastic *t* testing before calculating the p-values. Individual data points from each independent experiment (the number of the independent experiments is indicated in the figure legends) were used for the calculation of the significance.

Online supplemental material

Figs. S1 and S2 and Table S5 recapitulate the siRNA screen results for every individual virus. Fig. S3 shows the deconvolution experiments of the siRNA probes. Fig. S4 depicts the virus replication experiments upon ATG13 depletion. Fig. S5 and Table S6 resume the results of the MS analysis of FIP200 and ATG13 binding partners in CV-infected and uninfected cells. Fig. S6 shows the immunofluorescence- and EM-based localization studies of EMCV and CV replication structures. Tables S1 and S2 list the genes that are targeted in the siRNA screen. Table S3 lists the real-time PCR primers that were used in the study. Table S4 lists all the siRNA sequences used in this study. Table S7 collects all the RNA sequencing data. Online supplemental material is available at http://www.jcb.org/cgi/content/full/jcb.201602046/DC1.

Acknowledgments

The authors thank Lindsay Whitton, Xiaodong Wang, and Gert Strous for reagents; Daphne Lelieveld for assistance with laboratory automation; and Muriel Mari for assistance with electron microscopy. siRNA library management and automated microscopy were performed at the Cell Screening Core of the University Medical Centre Utrecht. RNA sequencing was performed in the Genome Analysis Facility of the University Groningen. We also thank Madelon Maurice and her group for comments and discussions. We are grateful to J.W. Harper for critical access to CompPASS.

F. Reggiori is supported by grants from the NWO Earth and Life Sciences (ALW) Open Program (822.02.014), Deutsche Forschungsgemeinschaft–Nederlandse Organisatie voor Wetenschappelijk Onderzoek cooperation (DN82-303), Schweizerischer Nationalfonds zur Förderung der Wissenschaftlichen Sinergia (CRSII3_154421), and Netherlands Organisation for Health Research and Development (ZonMW) VICI (016.130.606). S.A. Tooze is supported by Cancer Research UK and the Francis Crick Institute, which receives its core funding from Cancer Research UK, the UK Medical Research Council, and the Wellcome Trust. T. Ahola is supported by a grant from the Academy of Finland (265997). M. Langereis is supported by a grant from Nederlandse Organisatie voor Wetenschappelijk Onderzoek VENI (no. 863.13.008). F. van Kuppeveld is supported by a grant from Nederlandse Organisatie voor Wetenschappelijk Onderzoek VICI (918.12.628). J. Jung and C. Behrends are supported by grants from the Deutsche Forschungsgemeinschaft (BE 4685/1-1) and the European Research Council (282333). X. Zhou is supported by a Chinese Scholarship Council PhD fellowship.

The authors declare no competing financial interests.

Submitted: 15 February 2016
Accepted: 25 July 2016

References

Alirezaei, M., C.T. Flynn, M.R. Wood, and J.L. Whitton. 2012. Pancreatic acinar cell-specific autophagy disruption reduces coxsackievirus replication and pathogenesis in vivo. *Cell Host Microbe.* 11:298–305. http://dx.doi.org/10.1016/j.chom.2012.01.014

Alirezaei, M., C.T. Flynn, M.R. Wood, S. Harkins, and J.L. Whitton. 2015. Coxsackievirus can exploit LC3 in both autophagy-dependent and -independent manners in vivo. *Autophagy.* 11:1389–1407. http://dx.doi.org/10.1080/15548627.2015.1063769

Anders, S., P.T. Pyl, and W. Huber. 2015. HTSeq--a Python framework to work with high-throughput sequencing data. *Bioinformatics.* 31:166–169. http://dx.doi.org/10.1093/bioinformatics/btu638

Axe, E.L., S.A. Walker, M. Manifava, P. Chandra, H.L. Roderick, A. Habermann, G. Griffiths, and N.T. Ktistakis. 2008. Autophagosome formation from membrane compartments enriched in phosphatidylinositol 3-phosphate and dynamically connected to the endoplasmic reticulum. *J. Cell Biol.* 182:685–701. http://dx.doi.org/10.1083/jcb.200803137

Baker, J.M., and F.M. Boyce. 2014. High-throughput functional screening using a homemade dual-glow luciferase assay. *J. Vis. Exp.* 88:50282. http://dx.doi.org/10.3791/50282

Baron, M.H., and D. Baltimore. 1982. In vitro copying of viral positive strand RNA by poliovirus replicase. Characterization of the reaction and its products. *J. Biol. Chem.* 257:12359–12366.

Behrends, C., M.E. Sowa, S.P. Gygi, and J.W. Harper. 2010. Network organization of the human autophagy system. *Nature.* 466:68–76. http://dx.doi.org/10.1038/nature09204

Bestebroer, J., P. V'kovski, M. Mauthe, and F. Reggiori. 2013. Hidden behind autophagy: the unconventional roles of ATG proteins. *Traffic.* 14:1029–1041. http://dx.doi.org/10.1111/tra.12091

Bible, J.M., P. Pantelidis, P.K. Chan, and C.Y. Tong. 2007. Genetic evolution of enterovirus 71: epidemiological and pathological implications. *Rev. Med. Virol.* 17:371–379. http://dx.doi.org/10.1002/rmv.538

Blommaart, E.F., U. Krause, J.P. Schellens, H. Vreeling-Sindelárová, and A.J. Meijer. 1997. The phosphatidylinositol 3-kinase inhibitors wortmannin and LY294002 inhibit autophagy in isolated rat hepatocytes. *Eur. J. Biochem.* 243:240–246. http://dx.doi.org/10.1111/j.1432-1033.1997.0240a.x

Buckingham, E.M., J.E. Carpenter, W. Jackson, L. Zerboni, A.M. Arvin, and C. Grose. 2015. Autophagic flux without a block differentiates varicella-zoster virus infection from herpes simplex virus infection. *Proc. Natl. Acad. Sci. USA.* 112:256–261. http://dx.doi.org/10.1073/pnas.1417878112

Burkard, C., M.H. Verheije, O. Wicht, S.I. van Kasteren, F.J. van Kuppeveld, B.L. Haagmans, L. Pelkmans, P.J. Rottier, B.J. Bosch, and C.A. de Haan. 2014. Coronavirus cell entry occurs through the endo-/lysosomal pathway in a proteolysis-dependent manner. *PLoS Pathog.* 10:e1004502. (published erratum appears in *PLoS Pathog.* 2015. 11:e1004709) http://dx.doi.org/10.1371/journal.ppat.1004502

Chakrabarti, A., P.K. Ghosh, S. Banerjee, C. Gaughan, and R.H. Silverman. 2012. RNase L triggers autophagy in response to viral infections. *J. Virol.* 86:11311–11321. http://dx.doi.org/10.1128/JVI.00270-12

Chan, E.Y., S. Kir, and S.A. Tooze. 2007. siRNA screening of the kinome identifies ULK1 as a multidomain modulator of autophagy. *J. Biol. Chem.* 282:25464–25474. http://dx.doi.org/10.1074/jbc.M703663200

Chen, S., C. Wang, S. Yeo, C.C. Liang, T. Okamoto, S. Sun, J. Wen, and J.L. Guan. 2016. Distinct roles of autophagy-dependent and -independent functions of FIP200 revealed by generation and analysis of a mutant knock-in mouse model. *Genes Dev.* 30:856–869. http://dx.doi.org/10.1101/gad.276428.115

de Haan, C.A., L. van Genne, J.N. Stoop, H. Volders, and P.J. Rottier. 2003. Coronaviruses as vectors: position dependence of foreign gene expression. *J. Virol.* 77:11312–11323. http://dx.doi.org/10.1128/JVI.77.21.11312-11323.2003

Delorme-Axford, E., S. Morosky, J. Bomberger, D.B. Stolz, W.T. Jackson, and C.B. Coyne. 2014. BPIFB3 regulates autophagy and coxsackievirus B replication through a noncanonical pathway independent of the core initiation machinery. *MBio.* 5:e02147. http://dx.doi.org/10.1128/mBio.02147-14

De Palma, A.M., I. Vliegen, E. De Clercq, and J. Neyts. 2008. Selective inhibitors of picornavirus replication. *Med. Res. Rev.* 28:823–884. http://dx.doi.org/10.1002/med.20125

de Vries, E., D.M. Tscherne, M.J. Wienholts, V. Cobos-Jiménez, F. Scholte, A. García-Sastre, P.J. Rottier, and C.A. de Haan. 2011. Dissection of the influenza A virus endocytic routes reveals macropinocytosis as an alternative entry pathway. *PLoS Pathog.* 7:e1001329. http://dx.doi.org/10.1371/journal.ppat.1001329

Dorobantu, C.M., L. Albulescu, C. Harak, Q. Feng, M. van Kampen, J.R. Strating, A.E. Gorbalenya, V. Lohmann, H.M. van der Schaar, and F.J. van Kuppeveld. 2015. Modulation of the host lipid landscape to promote RNA virus replication: the picornavirus encephalomyocarditis virus converges on the pathway used by hepatitis C virus. *PLoS Pathog.* 11:e1005185. http://dx.doi.org/10.1371/journal.ppat.1005185

Eng, K.E., M.D. Panas, D. Murphy, G.B. Karlsson Hedestam, and G.M. McInerney. 2012. Accumulation of autophagosomes in Semliki Forest virus-infected cells is dependent on expression of the viral glycoproteins. *J. Virol.* 86:5674–5685. http://dx.doi.org/10.1128/JVI.06581-11

Eroglu, B., J.N. Min, Y. Zhang, E. Szurek, D. Moskophidis, A. Eroglu, and N.F. Mivechi. 2014. An essential role for heat shock transcription factor binding protein 1 (HSBP1) during early embryonic development. *Dev. Biol.* 386:448–460. http://dx.doi.org/10.1016/j.ydbio.2013.12.038

Fu, Y., W. Xu, D. Chen, C. Feng, L. Zhang, X. Wang, X. Lv, N. Zheng, Y. Jin, and Z. Wu. 2015. Enterovirus 71 induces autophagy by regulating has-miR-30a expression to promote viral replication. *Antiviral Res.* 124:43–53. http://dx.doi.org/10.1016/j.antiviral.2015.09.016

Glomb-Reinmund, S., and M. Kielian. 1998. The role of low pH and disulfide shuffling in the entry and fusion of Semliki Forest virus and Sindbis virus. *Virology.* 248:372–381. http://dx.doi.org/10.1006/viro.1998.9275

Hara, T., A. Takamura, C. Kishi, S. Iemura, T. Natsume, J.L. Guan, and N. Mizushima. 2008. FIP200, a ULK-interacting protein, is required for autophagosome formation in mammalian cells. *J. Cell Biol.* 181:497–510. http://dx.doi.org/10.1083/jcb.200712064

Hato, S.V., C. Ricour, B.M. Schulte, K.H. Lanke, M. de Bruijni, J. Zoll, W.J. Melchers, T. Michiels, and F.J. van Kuppeveld. 2007. The mengovirus leader protein blocks interferon-alpha/beta gene transcription and inhibits activation of interferon regulatory factor 3. *Cell. Microbiol.* 9:2921–2930. http://dx.doi.org/10.1111/j.1462-5822.2007.01006.x

He, C., and D.J. Klionsky. 2009. Regulation mechanisms and signaling pathways of autophagy. *Annu. Rev. Genet.* 43:67–93. http://dx.doi.org/10.1146/annurev-genet-102808-114910

Hieke, N., A.S. Löffler, T. Kaizuka, N. Berleth, P. Böhler, S. Drießen, F. Stuhldreier, O. Friesen, K. Assani, K. Schmitz, et al. 2015. Expression of a ULK1/2 binding-deficient ATG13 variant can partially restore autophagic activity in ATG13-deficient cells. *Autophagy.* 11:1471–1483. http://dx.doi.org/10.1080/15548627.2015.1068488

Hosokawa, N., T. Sasaki, S. Iemura, T. Natsume, T. Hara, and N. Mizushima. 2009. Atg101, a novel mammalian autophagy protein interacting with Atg13. *Autophagy.* 5:973–979. http://dx.doi.org/10.4161/auto.5.7.9296

Huang, S.C., C.L. Chang, P.S. Wang, Y. Tsai, and H.S. Liu. 2009. Enterovirus 71-induced autophagy detected in vitro and in vivo promotes viral replication. *J. Med. Virol.* 81:1241–1252. http://dx.doi.org/10.1002/jmv.21502

Huttlin, E.L., M.P. Jedrychowski, J.E. Elias, T. Goswami, R. Rad, S.A. Beausoleil, J. Villén, W. Haas, M.E. Sowa, and S.P. Gygi. 2010. A tissue-specific atlas of mouse protein phosphorylation and expression. *Cell.* 143:1174–1189. http://dx.doi.org/10.1016/j.cell.2010.12.001

Joo, J.H., F.C. Dorsey, A. Joshi, K.M. Hennessy-Walters, K.L. Rose, K. McCastlain, J. Zhang, R. Iyengar, C.H. Jung, D.F. Suen, et al. 2011. Hsp90-Cdc37 chaperone complex regulates Ulk1- and Atg13-mediated mitophagy. *Mol. Cell.* 43:572–585. http://dx.doi.org/10.1016/j.molcel.2011.06.018

Joo, J.H., B. Wang, E. Frankel, L. Ge, L. Xu, R. Iyengar, X. Li-Harms, C. Wright, T.I. Shaw, T. Lindsten, et al. 2016. The noncanonical role of ULK/ATG1 in ER-to-Golgi trafficking is essential for cellular homeostasis. *Mol. Cell.* 62:491–506. http://dx.doi.org/10.1016/j.molcel.2016.04.020

Jung, C.H., C.B. Jun, S.H. Ro, Y.M. Kim, N.M. Otto, J. Cao, M. Kundu, and D.H. Kim. 2009. ULK-Atg13-FIP200 complexes mediate mTOR signaling to the autophagy machinery. *Mol. Biol. Cell.* 20:1992–2003. http://dx.doi.org/10.1091/mbc.E08-12-1249

Jung, J., H.M. Genau, and C. Behrends. 2015. Amino Acid-Dependent mTORC1 Regulation by the Lysosomal Membrane Protein SLC38A9. *Mol. Cell. Biol.* 35:2479–2494. http://dx.doi.org/10.1128/MCB.00125-15

Kaizuka, T., and N. Mizushima. 2015. Atg13 is essential for autophagy and cardiac development in mice. *Mol. Cell. Biol.* 36:585–595. http://dx.doi.org/10.1128/MCB.01005-15

Kawamata, T., Y. Kamada, Y. Kabeya, T. Sekito, and Y. Ohsumi. 2008. Organization of the pre-autophagosomal structure responsible for autophagosome formation. *Mol. Biol. Cell.* 19:2039–2050. http://dx.doi.org/10.1091/mbc.E07-10-1048

Kemball, C.C., M. Alirezaei, C.T. Flynn, M.R. Wood, S. Harkins, W.B. Kiosses, and J.L. Whitton. 2010. Coxsackievirus infection induces autophagy-like vesicles and megaphagosomes in pancreatic acinar cells in vivo. *J. Virol.* 84:12110–12124. http://dx.doi.org/10.1128/JVI.01417-10

Kim, D., B. Langmead, and S.L. Salzberg. 2015. HISAT: a fast spliced aligner with low memory requirements. *Nat. Methods.* 12:357–360. http://dx.doi.org/10.1038/nmeth.3317

Kimmey, J.M., J.P. Huynh, L.A. Weiss, S. Park, A. Kambal, J. Debnath, H.W. Virgin, and C.L. Stallings. 2015. Unique role for ATG5 in neutrophil-mediated immunopathology during *M. tuberculosis* infection. *Nature.* 528:565–569. http://dx.doi.org/10.1038/nature16451

Klionsky, D.J., K. Abdelmohsen, A. Abe, M.J. Abedin, H. Abeliovich, A. Acevedo Arozena, H. Adachi, C.M. Adams, P.D. Adams, K. Adeli, et al. 2016. Guidelines for the use and interpretation of assays for monitoring autophagy (3rd edition). Autophagy. 12:1–222. http://dx.doi.org/10.1080/15548627.2015.1100356

König, R., S. Stertz, Y. Zhou, A. Inoue, H.H. Hoffmann, S. Bhattacharyya, J.G. Alamares, D.M. Tscherne, M.B. Ortigoza, Y. Liang, et al. 2010. Human host factors required for influenza virus replication. *Nature.* 463:813–817. http://dx.doi.org/10.1038/nature08699

Kroemer, G., G. Mariño, and B. Levine. 2010. Autophagy and the integrated stress response. *Mol. Cell.* 40:280–293. http://dx.doi.org/10.1016/j.molcel.2010.09.023

Laemmli, U.K. 1970. Cleavage of structural proteins during the assembly of the head of bacteriophage T4. *Nature.* 227:680–685. http://dx.doi.org/10.1038/227680a0

Landers, J.E., S.L. Cassel, and D.L. George. 1997. Translational enhancement of mdm2 oncogene expression in human tumor cells containing a stabilized wild-type p53 protein. *Cancer Res.* 57:3562–3568.

Langereis, M.A., Q. Feng, and F.J. van Kuppeveld. 2013. MDA5 localizes to stress granules, but this localization is not required for the induction of

type I interferon. *J. Virol.* 87:6314–6325. http://dx.doi.org/10.1128/JVI.03213-12

Lanke, K.H., H.M. van der Schaar, G.A. Belov, Q. Feng, D. Duijsings, C.L. Jackson, E. Ehrenfeld, and F.J. van Kuppeveld. 2009. GBF1, a guanine nucleotide exchange factor for Arf, is crucial for coxsackievirus B3 RNA replication. *J. Virol.* 83:11940–11949. http://dx.doi.org/10.1128/JVI.01244-09

Lee, Y.R., P.S. Wang, J.R. Wang, and H.S. Liu. 2014. Enterovirus 71-induced autophagy increases viral replication and pathogenesis in a suckling mouse model. *J. Biomed. Sci.* 21:80. http://dx.doi.org/10.1186/s12929-014-0080-4

Levine, B., and D.J. Klionsky. 2004. Development by self-digestion: molecular mechanisms and biological functions of autophagy. *Dev. Cell.* 6:463–477. http://dx.doi.org/10.1016/S1534-5807(04)00099-1

Levine, B., N. Mizushima, and H.W. Virgin. 2011. Autophagy in immunity and inflammation. *Nature.* 469:323–335. http://dx.doi.org/10.1038/nature09782

Li, F., T. Chung, and R.D. Vierstra. 2014. AUTOPHAGY-RELATED11 plays a critical role in general autophagy- and senescence-induced mitophagy in Arabidopsis. *Plant Cell.* 26:788–807. http://dx.doi.org/10.1105/tpc.113.120014

Li, H., B. Handsaker, A. Wysoker, T. Fennell, J. Ruan, N. Homer, G. Marth, G. Abecasis, and R. Durbin. 1000 Genome Project Data Processing Subgroup. 2009. The Sequence Alignment/Map format and SAMtools. *Bioinformatics.* 25:2078–2079. http://dx.doi.org/10.1093/bioinformatics/btp352

Limpens, R.W., H.M. van der Schaar, D. Kumar, A.J. Koster, E.J. Snijder, F.J. van Kuppeveld, and M. Bárcena. 2011. The transformation of enterovirus replication structures: a three-dimensional study of single- and double-membrane compartments. *MBio.* 2:e00166-11. http://dx.doi.org/10.1128/mBio.00166-11

Lu, Q., P. Yang, X. Huang, W. Hu, B. Guo, F. Wu, L. Lin, A.L. Kovács, L. Yu, and H. Zhang. 2011. The WD40 repeat PtdIns(3)P-binding protein EPG-6 regulates progression of omegasomes to autophagosomes. *Dev. Cell.* 21:343–357. http://dx.doi.org/10.1016/j.devcel.2011.06.024

Malhotra, R., J.P. Warne, E. Salas, A.W. Xu, and J. Debnath. 2015. Loss of Atg12, but not Atg5, in pro-opiomelanocortin neurons exacerbates diet-induced obesity. *Autophagy.* 11:145–154. http://dx.doi.org/10.1080/15548627.2014.998917

Mari, M., S.A. Tooze, and F. Reggiori. 2011. The puzzling origin of the autophagosomal membrane. *F1000 Biol. Rep.* 3:25. http://dx.doi.org/10.3410/B3-25

Meijer, A.J., and P. Codogno. 2004. Regulation and role of autophagy in mammalian cells. *Int. J. Biochem. Cell Biol.* 36:2445–2462. http://dx.doi.org/10.1016/j.biocel.2004.02.002

Mizushima, N., T. Noda, T. Yoshimori, Y. Tanaka, T. Ishii, M.D. George, D.J. Klionsky, M. Ohsumi, and Y. Ohsumi. 1998. A protein conjugation system essential for autophagy. *Nature.* 395:395–398. http://dx.doi.org/10.1038/26506

Mizushima, N., A. Yamamoto, M. Hatano, Y. Kobayashi, Y. Kabeya, K. Suzuki, T. Tokuhisa, Y. Ohsumi, and T. Yoshimori. 2001. Dissection of autophagosome formation using Apg5-deficient mouse embryonic stem cells. *J. Cell Biol.* 152:657–668. http://dx.doi.org/10.1083/jcb.152.4.657

Mizushima, N., B. Levine, A.M. Cuervo, and D.J. Klionsky. 2008. Autophagy fights disease through cellular self-digestion. *Nature.* 451:1069–1075. http://dx.doi.org/10.1038/nature06639

Moloughney, J.G., C.E. Monken, H. Tao, H. Zhang, J.D. Thomas, E.C. Lattime, and S. Jin. 2011. Vaccinia virus leads to ATG12–ATG3 conjugation and deficiency in autophagosome formation. *Autophagy.* 7:1434–1447. http://dx.doi.org/10.4161/auto.7.12.17793

Muehlenbachs, A., J. Bhatnagar, and S.R. Zaki. 2015. Tissue tropism, pathology and pathogenesis of enterovirus infection. *J. Pathol.* 235:217–228. http://dx.doi.org/10.1002/path.4438

Muthukrishnan, S., G.W. Both, Y. Furuichi, and A.J. Shatkin. 1975. 5′-Terminal 7-methylguanosine in eukaryotic mRNA is required for translation. *Nature.* 255:33–37. http://dx.doi.org/10.1038/255033a0

Ochiai, H., S. Sakai, T. Hirabayashi, Y. Shimizu, and K. Terasawa. 1995. Inhibitory effect of bafilomycin A1, a specific inhibitor of vacuolar-type proton pump, on the growth of influenza A and B viruses in MDCK cells. *Antiviral Res.* 27:425–430. http://dx.doi.org/10.1016/0166-3542(95)00040-S

Pelletier, J., and N. Sonenberg. 1988. Internal initiation of translation of eukaryotic mRNA directed by a sequence derived from poliovirus RNA. *Nature.* 334:320–325. http://dx.doi.org/10.1038/334320a0

Pirooz, S.D., S. He, T. Zhang, X. Zhang, Z. Zhao, S. Oh, D. O'Connell, P. Khalilzadeh, S. Amini-Bavil-Olyaee, M. Farzan, and C. Liang. 2014. UVRAG is required for virus entry through combinatorial interaction with the class C-Vps complex and SNAREs. *Proc. Natl. Acad. Sci. USA.* 111:2716–2721. http://dx.doi.org/10.1073/pnas.1320629111

Pohjala, L., A. Utt, M. Varjak, A. Lulla, A. Merits, T. Ahola, and P. Tammela. 2011. Inhibitors of alphavirus entry and replication identified with a stable Chikungunya replicon cell line and virus-based assays. *PLoS One.* 6:e28923. http://dx.doi.org/10.1371/journal.pone.0028923

Polson, H.E., J. de Lartigue, D.J. Rigden, M. Reedijk, S. Urbé, M.J. Clague, and S.A. Tooze. 2010. Mammalian Atg18 (WIPI2) localizes to omegasome-anchored phagophores and positively regulates LC3 lipidation. *Autophagy.* 6:506–522. http://dx.doi.org/10.4161/auto.6.4.11863

Reed, L.J., and H. Muench. 1938. A simple method of estimating fifty per cent endpoint. *Am. J. Epidemiol.* 27:493–497.

Reggiori, F., I. Monastyrska, M.H. Verheije, T. Calì, M. Ulasli, S. Bianchi, R. Bernasconi, C.A. de Haan, and M. Molinari. 2010. Coronaviruses Hijack the LC3-I-positive EDEMosomes, ER-derived vesicles exporting short-lived ERAD regulators, for replication. *Cell Host Microbe.* 7:500–508. http://dx.doi.org/10.1016/j.chom.2010.05.013

Ro, S.H., C.H. Jung, W.S. Hahn, X. Xu, Y.M. Kim, Y.S. Yun, J.M. Park, K.H. Kim, M. Seo, T.Y. Ha, et al. 2013. Distinct functions of Ulk1 and Ulk2 in the regulation of lipid metabolism in adipocytes. *Autophagy.* 9:2103–2114. http://dx.doi.org/10.4161/auto.26563

Rodriguez, J.F., D. Rodriguez, J.R. Rodriguez, E.B. McGowan, and M. Esteban. 1988. Expression of the firefly luciferase gene in vaccinia virus: a highly sensitive gene marker to follow virus dissemination in tissues of infected animals. *Proc. Natl. Acad. Sci. USA.* 85:1667–1671. http://dx.doi.org/10.1073/pnas.85.5.1667

Scheffner, M., K. Münger, J.C. Byrne, and P.M. Howley. 1991. The state of the p53 and retinoblastoma genes in human cervical carcinoma cell lines. *Proc. Natl. Acad. Sci. USA.* 88:5523–5527. http://dx.doi.org/10.1073/pnas.88.13.5523

Schneider, C.A., W.S. Rasband, and K.W. Eliceiri. 2012. NIH Image to ImageJ: 25 years of image analysis. *Nat. Methods.* 9:671–675. http://dx.doi.org/10.1038/nmeth.2089

Shintani, T., and D.J. Klionsky. 2004. Autophagy in health and disease: a double-edged sword. *Science.* 306:990–995. http://dx.doi.org/10.1126/science.1099993

Sowa, M.E., E.J. Bennett, S.P. Gygi, and J.W. Harper. 2009. Defining the human deubiquitinating enzyme interaction landscape. *Cell.* 138:389–403. http://dx.doi.org/10.1016/j.cell.2009.04.042

Subramani, S., and V. Malhotra. 2013. Non-autophagic roles of autophagy-related proteins. *EMBO Rep.* 14:143–151. http://dx.doi.org/10.1038/embor.2012.220

Sullivan, P.M., X. Zhou, A.M. Robins, D.H. Paushter, D. Kim, M.B. Smolka, and F. Hu. 2016. The ALS/FTLD associated protein C9orf72 associates with SMCR8 and WDR41 to regulate the autophagy-lysosome pathway. *Acta Neuropathol. Commun.* 4:51. http://dx.doi.org/10.1186/s40478-016-0324-5

Suzuki, H., T. Kaizuka, N. Mizushima, and N.N. Noda. 2015a. Structure of the Atg101-Atg13 complex reveals essential roles of Atg101 in autophagy initiation. *Nat. Struct. Mol. Biol.* 22:572–580. http://dx.doi.org/10.1038/nsmb.3036

Suzuki, S.W., H. Yamamoto, Y. Oikawa, C. Kondo-Kakuta, Y. Kimura, H. Hirano, and Y. Ohsumi. 2015b. Atg13 HORMA domain recruits Atg9 vesicles during autophagosome formation. *Proc. Natl. Acad. Sci. USA.* 112:3350–3355. http://dx.doi.org/10.1073/pnas.1421092112

Tabor-Godwin, J.M., G. Tsueng, M.R. Sayen, R.A. Gottlieb, and R. Feuer. 2012. The role of autophagy during coxsackievirus infection of neural progenitor and stem cells. *Autophagy.* 8:938–953. http://dx.doi.org/10.4161/auto.19781

Tebruegge, M., and N. Curtis. 2009. Enterovirus infections in neonates. *Semin. Fetal Neonatal Med.* 14:222–227. http://dx.doi.org/10.1016/j.siny.2009.02.002

Ulferts, R., L. van der Linden, H.J. Thibaut, K.H. Lanke, P. Leyssen, B. Coutard, A.M. De Palma, B. Canard, J. Neyts, and F.J. van Kuppeveld. 2013. Selective serotonin reuptake inhibitor fluoxetine inhibits replication of human enteroviruses B and D by targeting viral protein 2C. *Antimicrob. Agents Chemother.* 57:1952–1956. http://dx.doi.org/10.1128/AAC.02084-12

van der Linden, L., L. Vives-Adrián, B. Selisko, C. Ferrer-Orta, X. Liu, K. Lanke, R. Ulferts, A.M. De Palma, F. Tanchis, N. Goris, et al. 2015. The RNA template channel of the RNA-dependent RNA polymerase as a target for development of antiviral therapy of multiple genera within a virus family. *PLoS Pathog.* 11:e1004733. http://dx.doi.org/10.1371/journal.ppat.1004733

van der Schaar, H.M., P. Leyssen, H.J. Thibaut, A. de Palma, L. van der Linden, K.H. Lanke, C. Lacroix, E. Verbeken, K. Conrath, A.M. Macleod, et al. 2013. A novel, broad-spectrum inhibitor of enterovirus replication that targets host cell factor phosphatidylinositol 4-kinase IIIβ. *Antimicrob. Agents Chemother.* 57:4971–4981. http://dx.doi.org/10.1128/AAC.01175-13

Velikkakath, A.K., T. Nishimura, E. Oita, N. Ishihara, and N. Mizushima. 2012. Mammalian Atg2 proteins are essential for autophagosome formation and important for regulation of size and distribution of lipid droplets. *Mol. Biol. Cell.* 23:896–909. http://dx.doi.org/10.1091/mbc.E11-09-0785

Verheije, M.H., M. Raaben, M. Mari, E.G. Te Lintelo, F. Reggiori, F.J. van Kuppeveld, P.J. Rottier, and C.A. de Haan. 2008. Mouse hepatitis coronavirus RNA replication depends on GBF1-mediated ARF1 activation. *PLoS Pathog.* 4:e1000088. http://dx.doi.org/10.1371/journal.ppat.1000088

Wessels, E., D. Duijsings, R.A. Notebaart, W.J. Melchers, and F.J. van Kuppeveld. 2005. A proline-rich region in the coxsackievirus 3A protein is required for the protein to inhibit endoplasmic reticulum-to-golgi transport. *J. Virol.* 79:5163–5173. http://dx.doi.org/10.1128/JVI.79.8.5163-5173.2005

Wicht, O., C. Burkard, C.A. de Haan, F.J. van Kuppeveld, P.J. Rottier, and B.J. Bosch. 2014. Identification and characterization of a proteolytically primed form of the murine coronavirus spike proteins after fusion with the target cell. *J. Virol.* 88:4943–4952. http://dx.doi.org/10.1128/JVI.03451-13

Wong, J., J. Zhang, X. Si, G. Gao, I. Mao, B.M. McManus, and H. Luo. 2008. Autophagosome supports coxsackievirus B3 replication in host cells. *J. Virol.* 82:9143–9153. http://dx.doi.org/10.1128/JVI.00641-08

Wong, P.M., C. Puente, I.G. Ganley, and X. Jiang. 2013. The ULK1 complex: sensing nutrient signals for autophagy activation. *Autophagy.* 9:124–137. http://dx.doi.org/10.4161/auto.23323

Yakoub, A.M., and D. Shukla. 2015. Basal autophagy is required for herpes simplex virus-2 infection. *Sci. Rep.* 5:12985. http://dx.doi.org/10.1038/srep12985

Yang, Z., and D.J. Klionsky. 2010. Mammalian autophagy: core molecular machinery and signaling regulation. *Curr. Opin. Cell Biol.* 22:124–131. http://dx.doi.org/10.1016/j.ceb.2009.11.014

Zhang, H., C.E. Monken, Y. Zhang, J. Lenard, N. Mizushima, E.C. Lattime, and S. Jin. 2006. Cellular autophagy machinery is not required for vaccinia virus replication and maturation. *Autophagy.* 2:91–95. http://dx.doi.org/10.4161/auto.2.2.2297

Zhang, Y., Z. Li, X. Ge, X. Guo, and H. Yang. 2011. Autophagy promotes the replication of encephalomyocarditis virus in host cells. *Autophagy.* 7:613–628. http://dx.doi.org/10.4161/auto.7.6.15267

Zhao, Z., L.B. Thackray, B.C. Miller, T.M. Lynn, M.M. Becker, E. Ward, N.N. Mizushima, M.R. Denison, and H.W. Virgin IV. 2007. Coronavirus replication does not require the autophagy gene ATG5. *Autophagy.* 3:581–585. http://dx.doi.org/10.4161/auto.4782